ACS APPLIED MATERIALS & INTERFACES

Applications of Polymer, Composite, and Coating Materials

In-situ recyclable SERS-based detection of multicomponent pesticide residues on fruits and vegetables by flower-like MoS@Ag hybrid substrate

Ying Chen, Hongmei Liu, Yiran Tian, Yuan yuan Du, Yi Ma, Shuwen Zeng, Chenjie Gu, Tao Jiang, and Jun Zhou

ACS Appl. Mater. Interfaces, **Just Accepted Manuscript** • DOI: 10.1021/acsami.9b22725 • Publication Date (Web): 02 Mar 2020

In-situ recyclable SERS-based detection of multicomponent pesticide residues on fruits and vegetables by flower-like MoS_2@Ag hybrid substrate

Ying Chen,[†] Hongmei Liu,[‡] Yiran Tian,[†] Yuanyuan Du,[†] Yi Ma,[†] Shuwen Zeng,[§] Chenjie Gu,*[,†] Tao Jiang,*[,†] and Jun Zhou[†]

[†]Department of Microelectronic Science and Engineering, School of Physical Science and Technology, Ningbo University, Ningbo 315211, Zhejiang, P. R. China

[‡]Institute of Solid State Physics, Shanxi Datong University, Datong 037009, Shanxi, P. R. China

[§]XLIM Research Institute, UMR 7252 CNRS/University of Limoges, Avenue Albert Thomas, 87060, Limoges, France

*Corresponding author: jiangtao@nbu.edu.cn (T.J.) and guchenjie@nbu.edu.cn (C.G.).

ABSTRACT: Pesticides, extensively used in agriculture production, have received enormous attention because of their potential threats to the environment and human health. Hence, in this study, a kind of high sensitive and stable hybrid SERS-active substrates constructed with flower-like two-dimensional molybdenum sulfide and Ag (MoS_2@Ag) has been developed, and then the above substrate was sequentially utilized in the recyclable detection of pesticide residues on several kinds of fruits and vegetables. In the first place, the excellent photocatalytic performance of the MoS_2@Ag hybrid substrate was demonstrated, which was attributed to the inhibition of electron-hole combination after the formation of Schottky barrier between Ag NPs and MoS_2 matrix. Thereafter, two calibration curves with ultra-low limits of detection (LOD) as 6.4×10^{-7} and 9.8×10^{-7} mg/mL were established for the standard solutions of thiram (tetramethylthiuramdisulfide, TMTD) and methyl parathion (MP), and then the recyclable assay of their single and mixed residues on eggplant, Chinese cabbage, grape, and strawberry were successfully realized, respectively. It is interesting to note that the detection recoveries from 95.5% to 63.1% for TMTD and 92.3% to 62.6% for MP are greatly dependent on the size and surface roughness of these foods. In a word，the MoS_2@Ag composite matrix shows attractive SERS and photocatalysis performance, and it is expected to have the potential application on food safety monitoring.

KEYWORDS: flower-like MoS_2@Ag hybrid, SERS, photocatalysis, recyclable detection, pesticide residues

1. Introduction

Pesticides have been excessively used in nearly all kinds of vegetables and fruits to protect them against the harm from diseases, pests, and weeds. To be honest, the utilization of pesticides in agriculture has greatly improved the farm productivity as well as the quality of crops.[1] Nevertheless, the overusing of various pesticides at different stages of the crops has brought in severe residues on them, consequently inducing unavoidable hazard to ecological system and human health.[2] On the other hand, different kinds of vegetables and fruits maintain diverse sizes and surface roughnesses, which challenges the practical inspection of pesticide residues on them a lot. Therefore, it is imperative to develop a simple, rapid, efficient and reliable strategy with multi-component detection ability that can accurately in-situ monitor the mixed pesticide residues on daily foods.

To achieve the aforementioned purposes, plenty of laboratory analytical methods have been applied to detect and analyze pesticide residues on foods, including gas chromatography mass spectroscopy (GC-MS),[3] liquid chroma-tography mass spectroscopy (LC-MS),[4] high performance liquid chromatography (HPLC),[5] fluorescence spectroscopy,[6] and immunoassays.[7] Nevertheless, these methods present several disadvantages, including complicated sample treatment and time consuming, which hinder their wide use in the practical application. Thus, from the view point of making it easier and faster to monitor pesticide residues on food, it is desirable to develop alternative schemes, which are more suitable for accurate detection of multi-molecules with appreciated sensitivity, selectivity and efficiency. Among the reported

methods, surface-enhanced Raman scattering (SERS) has been considered as one of the most promising strategies, which possesses unique fingerprint spectrum, nondestructive data acquisition, and ultra-high sensitivity of even single molecule level.[8-10] And particularly, attributed to its narrow spectral linewidth, multiplexed in-situ testing can be easily realized in SERS detection. Therefore, SERS technique has been extensively used in the assay of various pesticide residues on vegetables and fruits.

It is generally acknowledged that the high sensitivity of SERS technology mainly depends on the choice of SERS-active materials as well as their unique structure, therefore, in the past decades, extensive researches have been performed on noble metal nanoparticles (Ag or Au NPs) with different structures to obtain high-active SERS substrates.[11] However, the reproducibility of noble metal NPs with prominent property is strongly dependent on the reliability of the chemical preparation process, which is usually a little poor and severely restricts their wide applications. So as to obtain much more facile and efficient synthesis method, some physical deposition strategies have been developed, such as magnetron sputtering.[12] The superior of this method lies in the fact that not only its preparation process is simple, but also it maintains high repeatability, by which the size and density of noble metal nanomaterials can be accurately controlled through adjusting the sputtering time and power. Besides the exploitation of more powerful physical technology, the construction of self-cleaning composite substrates through introducing semiconductor materials with photocatalytic activity is another novel alternative strategy to achieve the reusing of noble metal nanomaterials.[13-15] At the same time, it is still urgent to demonstrate multifunctional

nanocomposites, which can not only sensitively monitor but also efficiently degrade the environmental pollutions.[14] For these reasons, many research efforts have been recently focused on the preparation of recyclable SERS substrates.

MoS_2, a layered transition metal dichalcogenides, has gained an increasing level of attention for inexpensive price, good stability, and potential catalytic properties.[16-18] Nevertheless, the difficulty in separating the photo-generated electron-hole pairs in MoS_2 leads to low photocatalytic efficiency, preventing its broad applications.[19] With the aim to retard the recombination of electron-hole pairs for promoting the photocatalytic efficiency, one of the most effective methods is to introduce extra trapping center for the excited electrons through utilizing noble metal NPs. For example, compared with bare MoS_2, Ag NPs modified MoS_2 nanoflakes exhibited a higher hydrogen gas evolution attributed to the "pool" role of Ag NPs to gather photo excited-electrons and suppress their recombination.[19] Similarly, Cr NPs have also been anchored onto the surface of MoS_2 nanosheets together with Ag as trapping sites by a solution-based method to enhance the photocatalytic hydrogen evolution performance of MoS_2 nanosheets alone.[20] The introduction of noble metal here can not only improve the photocatalytic efficiency of MoS_2, but also induce a variety of nanocomposites to be used as SERS substrates with ultra-high sensitivity. For instance, a novel MoS_2@Au nanocomposite has been proposed by a spontaneous redox reaction induced by the MoS_2 matrix itself without the addition of reducing agent and a limit of detection (LOD) as low as 1.0×10^{-6} M was revealed.[16] Another Ag-MoS_2 nanohybrid prepared by photochemical reduction of femtosecond laser pulses has exhibited a SERS

enhancement factor (EF) of 1.32×10^7 with a LOD low to 1.0×10^{-11} M.[18] Such EF of SERS has been further improved to 1.2×10^8 by a plasmonic 3D MoS_2-NS@Ag-NP nanostructure prepared through an interfacial self-assembly technology together with a seeded growth strategy, and as a result, the LOD of 10 ppb for trace thiram in apple juice and local lake water was realized.[21] Moreover, the LOD of Rhodamine 6G was even extended to 1.0×10^{-12} and 1.0×10^{-14} M by utilizing Au NPs decorated MoS_2 nanoflowers and AuNPs/GO@MoS_2/AuNPs nanostructures, respectively.[22-23] At this stage, it is worth to mention that the dominant contributions of MoS_2 in the above SERS substrate can be ascribed to its three distinctive characters. Firstly, the high specific surface area of MoS_2 nanosheets offer abundant anchoring sites for noble metal NPs, which subsequently support the enrichment of molecules during the SERS detection. Secondly, MoS_2 can isolate highly active noble metal NPs from air, preventing them from getting oxidized, and consequently the hybrid substrate can be preserved for a long time. Finally, the as-obtained MoS_2 usually maintains irregular shape with large amount of corrugated and creviced regions, when noble metal NPs were densely attached onto these regions, substantial SERS "hot spots" could emerge on the substrate. However, it should be noted that there have been very limited applications of their photocatalytic activity in these practical SERS detections. In particular, to our knowledge, there is nearly no systematically investigation about the dependence of SERS activity and photocatalytic efficiency on the amount of decorated Ag NPs on MoS_2 matrix. And these innovative multifunctional and reusable SERS platforms have

rarely been applied for in-situ recyclable detection of pesticides on fruits and vegetables with diverse sizes and surface roughnesses.

Herein, a hybrid semiconductor-noble metal substrate with admirable SERS activity and photocatalytic efficiency was prepared by magnetron sputtering Ag NPs onto hydrothermal synthesized flower-like MoS_2 nanomaterials. And the recyclable SERS-based monitoring scheme of multicomponent pesticide residues on several kinds of fruits and vegetables with different sizes and surface roughnesses was developed sequentially. Firstly, the coverage amount of Ag NPs on the surface of MoS_2 matrix was adjusted by changing sputtering time and power, and the influence of Ag coating on their SERS performance and photocatalytic activity was studied systematically. Secondly, the flower-like MoS_2@Ag substrate with the optimal properties was utilized in the recyclable SERS-based detection of thiram (tetramethylthiuramdisulfide, TMTD) and MP (methyl parathion) in their standard solutions, respectively. And especially, two corresponding linear dose-response curves with wide detection ranges from 1.0×10^{-1} to 1.0×10^{-6} and from 1.0×10^{-1} to 2.5×10^{-6} mg/mL were successfully established. Then, the trace TMTD and MP residues on eggplant, Chinese cabbage, grape, and strawberry were examined by the as-obtained recyclable SERS-active substrate based on the above two linear dose-response curves. The detection recoveries ranged from 95.5% to 63.1% for TMTD and 92.3% to 62.6% for MP, respectively. Finally, the multicomponent detection ability of the hybrid substrate was demonstrated by monitoring the TMTD and MP with different mixed concentration ratios. All in all, this work presents a quantitative and highly sensitive recyclable SERS-based detection of

trace pesticide residues in real samples, facilitated by the multifunctional flower-like MoS_2@Ag hybrid substrate, and it is expected to be able to provide a low-cost and high efficient approach for future application on food safety monitoring.

2. Experimental

2.1 Materials

Sodium molybdate dihydrate ($Na_2MoO_4 \cdot 2H_2O$, 99%), thioacetamide (C_2H_5NS, 99%), and TMTD ($C_6H_{12}N_2S_4$, 97%) were purchased from Macklin Biochemical Co., Ltd. Tungstosilicic acid hydrate ($H_4Si[W_3O_{10})_4] \cdot xH_2O$), methanol solution of MP (1 mg/mL), and 4-mercaptobenzoic acid (4MBA, 90%) were obtained from Aladdin Biochemical Technology Co., Ltd. Sodium hydroxide (NaOH), methanol (CH_3OH), and ethanol (CH_3CH_2OH, ≥99.7%) were purchased from Sinopharm Chemical Reagent Co., Ltd. Milli-Q water (18.2 MΩ·cm) was used in the preparation of samples. All chemicals used in this work were of analytic purity and used without further purification.

2.2 Preparation of Flower-Like MoS_2@Ag Hybrid Substrate

The flower-like MoS_2 matrix was synthesized by a facile hydrothermal method.[24] 3 mmol of $Na_2MoO_4 \cdot 2H_2O$, 9 mmol of CH_3CSNH_2, and 2.8 mmol of $H_4Si[W_3O_{10})_4] \cdot xH_2O$ were mixed in 50 mL of deionized water under violent stirring. After the reaction reagents were dissolved well, a moderate amount of NaOH aqueous solution (1 M) were used to adjust the pH value of the above solution to 7.6. Then, the precursor solution was added into a hydrothermal autoclave, which was sealed and kept at 220 ℃ for 24 h. After it was cooled, and the resulted samples were filtered off and

subsequently cleaned with NaOH solutions, absolute ethanol, and deionized water. Finally, the purified products were dried under vacuum condition at 60 ℃ for 6 h.

In the preparation of MoS_2@Ag hybrid substrate, 10 mg of MoS_2 powder was dissolved in 1 mL of purified water to form homogeneous solution. Then, 20 μL of the above solution was dropped onto clean silicon wafers and dried naturally in air. After that, Ag NPs were coated onto the as-prepared MoS_2 matrix by sputtering an Ag target (99.99%) in a radio-frequency magnetron sputtering system, which operated at 0.3 Pa with the working power of 50 W in an ambient of Ar. The sputtering time was tuned from 60, 80, 100, 120 to 140 s, respectively. After sputtering deposition, the obtained Ag-decorated MoS_2 substrate was finally stored under vacuum condition for further test.

2.3 Detection of 4MBA, TMTD, and MP by the Flower-Like MoS_2@Ag Hybrid Substrate

4MBA was chosen as the Raman model probe to test the feasibility of flower-like MoS_2@Ag hybrid substrate, which was then used to detect the standard solutions of TMTD and MP molecules. In brief, 20 μL of 4MBA, TMTD, and MP solutions with different concentrations were carefully dropped onto the obtained substrate, and then the SERS spectra were measured after the substrates were naturally evaporated at room temperature for 2 h to ensure the binding of pesticide molecules.

2.4 Detection of Pesticide Residues on Foods

The fruits and vegetables including eggplant, Chinese cabbage, grape, and strawberry were washed with deionized water carefully. Then, 20 μL mixture solutions of the

TMTD and MP molecules with various concentration ratios were dropped onto the peels of the above vegetables and fruits and evaporated naturally at room temperature. After the TMTD and MP molecules from the pretreated peels were extracted by utilizing ethanol and methanol solutions, the SERS-active substrate was applied to slowly and carefully swab the surfaces of the peels. Finally, the SERS substrate was placed at room temperature for more than 2 h to ensure the binding of pesticide molecules for following SERS analysis.

2.5 Photocatalysis and Recyclable SERS-Based Detection

After the linking of 4MBA or pesticide residues onto the as-obtained flower-like MoS_2@Ag substrate, a SERS-based direct detection of 4MBA or pesticide residues was carried out, and all SERS spectra were recorded by averaging five measurement data. After that, the substrate was illuminated by an ultraviolet light (365 nm, 50 W) for a certain time to realize the photocatalytic degradation of 4MBA or pesticide molecules. During this period, the degradation of the molecules was monitored by measuring the corresponding SERS spectra every 20 min until the Raman signals are undetectable. Thereafter, the substrate was washed for several times with deionzied water and reused for the second detection and photocatalysis of the molecules. The above cyclical detection and photocatalysis were repeated until the LOD of the target molecules was reached as illustrated in Scheme 1.

2.6 Characterizations.

The morphologies of the samples were examined by using a field emission scanning electron microscope (FESEM, SU-70, Hitachi). Transmission electron microscopy

(TEM) and high-resolution TEM images, selective area electron diffraction (SAED) pattern, and energy-dispersive X-ray analysis (EDAX) were obtained from an electron microscope (Tecnai G2 F20, FEI) to characterize the structure, crystal phase, and component of the samples. The crystalline structure of the products could also be investigated by an X-ray power diffractometer (D8 ADVANCE, Bruker,). The deposition of Ag NPs on the MoS_2 matrix was carried out by a magnetron sputtering device (TA13-XD) at a pressure of 0.3 Pa and a power of 50 W. The absorption spectra of the sample during the photocatalysis process were recorded using the ultraviolet-visible (UV-vis) spectrometer (TU-1901, Pgeneral). X-ray photoelectron spectroscopy (XPS) was measured using an Al Ka X-ray source with an operating power of 150 W. SERS data were acquired with a Raman spectrometer equipped with a microscope with a 50 × objective lens (QE Pro, Ocean Optics) at the excitation wavelength of 532 nm. The laser power at the sample position was about 17 mW and the accumulation time was 10 s. The photocatalysis of the molecules on the sample was conducted by using a 365-nm LED UV light with 50 W output powder (HY-UV365-P).

3 Results and discussion

3.1 Characterization of the MoS_2 Matrix

In literatures, MoS_2 nanomaterials with high yield are usually synthesized by hydrothermal method without using harmful gases and extremely high reaction temperature.[16,22,24] The resulted samples can be well dispersed in solutions and stably exist in atmospheric environments without surfactants or oxidation treatment. And

particularly, the morphology of MoS_2 can be well adjusted by easily tuning the reaction parameters. Herein, such a facile hydrothermal method was also used to fabricate the MoS_2 matrix. Although a long washing period was required, there is in fact no strong surfactants on the samples. Only NaOH solutions, absolute ethanol, and deionized water were utilized without using any special hazardous washing reagents, resulting in a green synthetic process. As depicted in Figure 1a, MoS_2 nanostructures with flower-like morphologies were successfully synthesized in a high yield. The distribution of the diameter is in the range of 445 to 735 nm. The magnified SEM image of one typical MoS_2 nanoflower is shown in Figure 1b, and as it can be seen that MoS_2 nanoflower is composed of numerous nano-petals with the thickness of 1 to 1.5 nm, for which the thickness variations are ascribed to the MoS_2 layer number difference, and these nano-petals self-assemble into the 3D nanostructures.[22] EDS of MoS_2 is shown in Figure S1, the quantification of the yellow stripe shows that the atomic ratio of S to Mo is about 2.12, which is basically consistent with the stoichiometric of MoS_2. Meanwhile, this hierarchical nanoflowers create relative large surface areas for later Ag modification. The TEM image in Figure 1c further presents the composed nanosheets of the MoS_2 nanoflowers, which are ultra-thin with several sharp edges. The crystal structure of MoS_2 was then studied by HRTEM image and SAED pattern. The inter-layer spacing of 0.611 nm can be clearly observed as illustrated in Figure 1d, which is consistent with the (002) plane of hexagonal MoS_2. And two diffraction rings in Figure 1e can be identified and assigned to the (103) and (110) planes of MoS_2, respectively.

3.2 Characterization of the Flower-Like MoS_2@Ag Hybrid Substrate

Morphologies of flower-like MoS_2@Ag hybrid substrates synthesized with different Ag sputtering times were characterized by SEM and the typical images are shown in Figure 2. When the sputtering time was initially set to 60 s, a relatively sparse layer of Ag NPs can be found on the nanoflowers, and the sheet structure of MoS_2 could still be clearly observed as shown in Figure 2a, b. With the further increase of the sputtering time from 80 to 100 s, the MoS_2 matrix was gradually covered by more and more Ag NPs until a uniform thin coating layer formed as presented in Figure 2c-f. Afterwards, it can be seen from Figure 2g, h that there is nearly no exposed surface of MoS_2 when the sputtering time was extended to 120 s. However, the characteristic 3D hierarchical structures still maintains. Finally, when the sputtering time reached 140 s, a plethora of deposited Ag NPs assembled with each other, resulting in a large amount of aggregations and an irregular surface architecture. Based on the above experimental trace, it is clear that the sputtering time of Ag is a key factor that affects the morphology of the composite substrate. Other than that, the EDS was measured to confirm the composition of elements and their relative contents in the typical flower-like MoS_2@Ag substrate prepared with the sputtering time of 100 s. As illustrated in Figure S2a, with the exception of the original Mo, S element, the appearance of Ag peaks gives clear evidence of the successful modification of Ag layer on MoS_2. After that, the phase purity and crystal structure of the bare MoS_2 and MoS_2@Ag hybrid substrates were systematically explored by using the XRD analysis. As it is shown in Figure S2b, all peaks of MoS_2 can be indexed into (002), (100), (103), and (110) planes of hexagonal phase (JCPDS 37-1492) without residues or impurity phases, indicating the complete

sulfuration of MoO_4^{2-}. And after the magnetron sputtering, characteristic peaks from the (111) and (200) planes of cubic face centered Ag appear in XRD pattern and their intensities continually climbs, indicating the enrichment of Ag content with the extension of sputtering time. Besides, the featured XRD peaks of MoS_2 in the hybrid substrate are similar to those of the bare MoS_2, which suggests that the modification of the Ag NPs have no influence on their crystalline structure.

TEM, HRTEM, SAED, and EDX elemental mapping was then utilized to discern the structure and crystal phase of the hybrid substrate as illustrated in Figure 3. It is clearly identified from Figure 3a that the MoS_2 matrix presents a well-layered structure, and Ag NPs can be found to adhere at the edge of the nanosheets, confirming the formation of MoS_2@Ag hybrid structure. Then, the HRTEM images in Figure 3b, c detect several selected regions of MoS_2 and Ag, and they reveal that the interplanar spacing of approximately 0.234 and 0.611 nm, which corresponds to the (111) plane of Ag and (002) plane of MoS_2, respectively. Moreover, it can be concluded from the SAED pattern of the matrix (Figure 3d) that except the initial diffraction rings of MoS_2, the single crystalline structure of the deposited Ag NPs could be identified by the bright diffraction pots, which can be assigned to the allowed (111) and (200) reflections, respectively. In addition, EDX elemental mapping analyses (Figure 3e) illustrate the distribution of Mo, S, and Ag elements in the substrate, further revealing its hybrid structure and the uniform deposition of Ag NPs on the MoS_2 matrix. To further qualitatively and quantitatively reveal the chemical states of each element in the MoS_2@Ag substrate, the XPS characterizations were carried out as shown in Figure 4.

All of the element spectra were calibrated by a carbon 1 s peak (284.7 eV). The survey spectrum of MoS_2@Ag composites as depicted in Figure 4a demonstrates the presence of Mo, S, and Ag elements. Two well-defined peaks at 367.5 and 373.5 eV in the spectrum of Ag 3d with high resolution are attributed to Ag $3d_{5/2}$ and Ag $3d_{3/2}$ which derived from the sputtered Ag NPs (Figure 4b). Meanwhile, in the fine spectrum of Mo 3d (Figure 4c), two peaks at 228.2 and 231.3 eV can be assigned to Mo $3d_{5/2}$ and Mo $3d_{3/2}$, which suggest the IV oxidation state of Mo is dominant in the MoS_2 matrix. Besides, the peak at 225.6 eV is attributed to S 2s, and the peak at 235.6 eV is due to Mo-O bond caused by the oxidation of the MoS_2 surface.[25-26] Additionally, in the high-resolution S 2p spectrum (Figure 4d), it can be seen that there are two peaks of S $2p_{1/2}$ at 162.0 eV and S $2p_{3/2}$ at 161.1 eV, which can be assigned to the S^{2-}. In brief, the above characterizations confirm the final obtaining of the MoS_2@Ag hybrid substrate, which could be utilized in the following practical SERS-based detections.

3.3 SERS Property and Photocatalytic Activity of the Flower-Like MoS_2@Ag Hybrid Substrate

Attributed to the fact that it can easily chemisorb on the surface of noble metal NPs through Ag (Au)–S bonds, 4MBA has been extensively exploited as a model molecule to realize reproducible output of SERS signals.[27] Therefore, 4MBA was also used in this work to investigate the SERS performance of the samples. The averaged SERS spectra of 4MBA molecules from the bare MoS_2 matrix and various MoS_2@Ag hybrid substrates prepared with diverse sputtering times of Ag NPs are compared in Figure 5a. The almost negligible characteristic peaks of 4MBA at 1078 and 1587 cm^{-1} from the

bare MoS_2 matrix are gradually triggered after the decoration of more and more Ag NPs. Such a boosting trend of the SERS intensity towards deposition amount of Ag NPs is more directly shown by presenting the average intensities of peak at 1587 cm^{-1} in Figure 5b. As it is known that size, density and aggregation degree of Ag NPs all play critical roles in obtaining high SERS activity. Considering the situation in our experiment, attributed to the rough surfaces with relative high area ratio of the hierarchical MoS_2 matrix, the significant aggregation of Ag NPs with appropriate interparticle spacing could form and be maintained on the matrix, which benefits the formation of the electromagnetic "hot spots". Additionally, the enrichment of Ag NPs on the surface of MoS_2 nanoflowers further raise the total number of effective 4MBA molecules on the noble metal, which will contribute to the overall Raman signal intensity.[28-31]

The SERS enhancement ability of the prepared flower-like MoS_2@Ag matrix was evaluated using the Raman EF, which is calculated by the following equations: $EF = (I_{SERS}/I_{Raman}) \times (N_{Raman}/N_{SERS})$, where I_{SERS} and I_{Raman} are the integrated intensity of SERS peaks at 1587 cm^{-1} of 4MBA on the hybrid matrix and that of the 4MBA powder on the glass substrate, respectively. N_{Raman} and N_{SERS} represent the molecule amounts of 4MBA bare powder and 4MBA molecules absorbed on the hybrid substrate within the illuminated area, respectively. In order to calculate N_{Raman}, the diameter of focus laser spot as 1.18 μm was calculated by applying the equation $D_{diamter} = (\lambda/NA) \times 1.22$, where λ is 532 nm and the value of the numerical aperture (NA) is 0.55. And the penetration depth of the focused beam into the 4MBA powder was estimated as 3.52

μm by the equation $D_{depth} = 2\lambda/NA^2$, resulting a volume of 1.28 μm^3. Considering the density and molecular weight of molecule power as 1.5 g cm^{-3} and 154.19 g mol^{-1}, N_{Raman} was calculated as 7.5×10^9. N_{SERS} was calculated by the equation: $N_{SERS} = N_A \times A/\delta$, where NA is Avogadro constant, A refers to the effective area of 4MBA molecules in the laser spot and its value is 0.55 μm^2. And the area of molecules per mole in a monolayer exhibits a δ of 2.0×10^{-9} cm^2 mol^{-1}.[32] Therefore, the value of N_{SERS} was calculated to be 1.66×10^6. At the same time, the values of I_{SERS} and I_{Raman} were recorded to be 9.9×10^5 and 3.9×10^3 according to integral area of SERS spectrum of 4MBA molecules absorbed on the SERS-active matrix and the Raman spectrum of 4MBA power (Figure S3). Eventually, EF value was obtained to be 1.1×10^6.

Besides the attractive SERS properties, the flower-like MoS_2@Ag hybrid substrate also possesses photocatalytic ability owing to the presence of MoS_2, which provides great opportunities for the realizing of recyclable SERS-based detection. In order to evaluate the photocatalytic activity of the substrates with different coating amounts of Ag NPs and explore the superior one, the photocatalytic degradation experiment were carried out on a series of substrates with 4MBA decoration. The SERS spectra versus time for these MoS_2@Ag hybrid substrates under UV light are illustrated in Figure 6a and Figure S4a-d. Obviously, a temporal drift of the 4MBA SERS signal can be visualized. The SERS signals from the MoS_2@Ag substrates synthesized with sputtering time of 60, 80, and 100 s become completely undetectable when the catalytic time extends to 125 min. On the contrary, noticeable SERS intensities still can be observed even when the UV irradiation reaches 130 min, manifesting the significant

residue of 4MBA on the substrates synthesized with longer sputtering times of 120 and 140 s. Henceforth, to further compare the degradation efficiency of the various hybrid substrates more directly, the SERS peak located at 1587 cm^{-1} was chose as a signature, and the corresponding time-dependent ratios of I/I_0 based on the above samples are shown in Figure 6b, where I_0 is the initial SERS intensity and I is the intensity after UV irradiation. It is evident that the substrate prepared with the sputtering time of 100 s shows the largest degradation slope, indicating its astonishing photocatalytic activity. However, as it also can be observed in Figure 6b that if UV irradiation was not performed, there is nearly no degradation of 4MBA. In addition, control experiment of irradiating 4MBA molecules in the absence of MoS_2@Ag substrate was also conducted. Although slight photothermal degradation of 4MBA was observed, it was almost negligible compared with that induced by photocatalysis. At this point, it is evidence that MoS_2 in the hybrid substrates play a critical role in achieving photocatalysis. Subsequently, in order to further reveal the crucial role of Ag NPs in enhancing the photocatalytic efficiency, Raman signal of 4MBA from bare MoS_2 matrix was also recorded. Unfortunately, without electromagnetic enhancement, the Raman signal is too weak to show the photocatalytic process obviously in the absence of Ag NPs. In this regard, the traditional liquid phase photocatalytic strategy was used as an alternative method to compare the photocatalytic efficiency of the bare MoS_2 matrix and that modified by Ag NPs. The as-prepared sample was carefully immersed into a small beaker containing 1 mM 4MBA solutions, a portion of which under UV irradiation was taken every 20 min to measure their UV-vis absorption spectra until no apparent

characteristic band of 4MBA at 273 nm was observed as represented in Figure 6c and S5. After 125 min of UV irradiation, the degradation rate of 4MBA by the MoS_2 matrix approaches to 96.3%, and the required degradation time of 4MBA by 96.9% adsorbed on the MoS_2@Ag hybrid substrate with sputtering time of 100 s decreased to 90 min, which is nearly 1.3 times shorter than bare MoS_2 matrix. These findings verify that the hybrid substrate maintains the significantly enhanced photocatalytic activity toward degradation of 4MBA. In the meanwhile, the corresponding time-dependent ratios of C/C_0 based on the different substrate of MoS_2 and MoS_2@Ag are shown in Figure 6d, where C_0 is the initial absorption intensity and C is the intensity after UV irradiation. From the absorption intensity degradation curve, it can be known that the hybrid substrate has better catalytic efficiency. Furthermore, in order to understand the mechanism for such improvement, a possible catalytic procedure is elucidated in Scheme 1. When the samples were exposed under photo-irradiation with appropriate photon energy, a large number of electrons (e^-) from the valence band of MoS_2 can be excited to the conduction band and leave holes (h^+) in valence band. These highly active electrons will be captured by the oxygen adsorbed on the surface of the nanocomposites and produce super oxide radicals ($\bullet O_2^-$). Meanwhile, the interactions between the corresponding holes and the surface H_2O will produce hydroxyl ($\bullet OH^-$). The detailed reaction process and the corresponding equations are illustrated below. With strong oxidant ability, these groups of $\bullet O_2^-$ and $\bullet OH^-$ can directly oxidize the target organic molecules.[14,33-34]

(1) $hv + MoS_2 \rightarrow MoS_2 (h^+ + e^-)$;

(2) $e^- + H_2O_2 \rightarrow OH^- + \bullet OH^-$;

(3) $e^- + O_2 \rightarrow \bullet O_2^-$;

(4) $h^+ + \bullet OH^- \rightarrow \bullet OH^- + H^+$.

However, in the intrinsic semiconductors including MoS_2, it is always difficult to separate the photo-generated electron-hole pairs effectively, resulting in low photocatalytic efficiency. In this regard, various semiconductors have been combined with noble metals to improve the practical performance of the former ones, and the proposed mechanisms of the enhancement of charge separations or photocatalytic efficiency are summarized in Table 1. The main reasons include the generation of "hot electrons" induced by plasma, the formation of Schottky barrier between noble metal and semiconductor, the good conductivity of noble metal or graphene etc. In this work, owing the band structures of Ag and MoS_2, the existence of Schottky barrier was also proposed to elucidate the mechanism of the better photocatalytic performance. It is known to all that work function is defined as the distance between vacuum level and Femi level as shown in the Figure S6a. Based on the previous experimental data, the work function of the modified Ag NPs dominated by (111) crystal plane is known as 4.74 eV [40] and those of MoS_2 range from 4.2 to 4.6 eV.[41] When the MoS_2 matrix with lower work function contact with the Ag NPs, Schottky barriers (the bending up of surface energy level in semiconductor) will form between them to reach the balance of Femi level, which facilitates the transfer of electrons from the semiconductor to the metal as shown in Figure S6b.[42] As a consequence, the modified Ag NPs, serving as acceptors of electrons, will effectively reduce the recombination of the photo-generated

electron-hole pairs. Nevertheless, too many Ag NPs will become the recombination center of electron-hole pairs, thereby reducing the photocatalytic activity of hybrid substrate.[43] Another possible reason for the reduction of the photocatalytic efficiency with more decorated Ag NPs is speculated that the formation of too thick Ag layers on the MoS_2 matrix will prevent the efficient interaction between the semiconductor and the target molecules. Based on these results, the MoS_2@Ag substrate synthesized with sputtering time of 100 s is expected to have optimum photocatalytic ability, endowing it great potential for practical recyclable assay.

3.4 Investigation of Sensitivity and SERS Stability

With the aim to conduct a practically recyclable SERS-based monitoring of trace pesticide residues in fruit and vegetable, sensitivity and reproducibility of the SERS substrate with the optimal photocatalysis property was then evaluated, which are two prerequisites to achieve the reliable ultrasensitive SERS detection. In the first place, the monitoring of 4MBA with different concentrations were performed on the flower-like MoS_2@Ag hybrid substrate synthesized with sputtering time of 100 s and the corresponding SERS spectra are shown in Figure 7a. It can be observed that the Raman signal is accordingly diminishing when the 4MBA solution is diluted from 1.0×10^{-4} to 1.0×10^{-10} M, and even when the concentration reaches 1.0×10^{-10} M, the Raman spectra still can be clearly identified. Additionally, blank control experiment was also conducted by collecting the spectrum from the bare substrate without Raman molecules, and the scarce signal indicates a negligible background interference in SERS-based detection. Thereafter, experimental data of the 4MBA fingerprint peak intensity at 1587

cm^{-1} and the molecule concentration were used to access the analytical relationship between them. As it is shown in Figure 7b, a well-defined linear relationship can be obtained, giving a R^2 value of 0.989. Particularly, the LOD of the substrate was estimated to be 5.9×10^{-11} M based on three times of the signal-to-noise ratio from the background spectrum.[44] Simultaneously, SERS mapping of the band at 1587 cm^{-1} from total 900 points on the 600×600 μm^2 portions of the hybrid substrate was collected as presented in Figure 7c. A small RSD value of only 14.9% was finally obtained due to the slight fluctuation of these SERS signals (Figure 7d). These results evidence that the excellent sensitivity and comparatively good uniformity assure the flower-like MoS_2@Ag hybrid substrate superior as a potential SERS matrix in practical applications.

In fact, the aggregation of Ag NPs during storage will to some extent affects their practical applications and especially the repeatability of SERS signal. Up to now, it remains great challenge to avoid the aggregation of Ag NPs with exposed surfaces.[23] The morphology and SERS stability of the flower-like MoS_2@Ag hybrid substrate were tested in air atmosphere at room temperature as shown in Figure 8. After being stored for one month, the hierarchical structure of the hybrid substrate could still be kept and no severe aggregation was observed as presented in Figure 8a, c. However, it is quite evident from magnified images that some minor Ag NPs on the substrate disappeared (Figure 8b, d), indicating the slight oxidization happens on the substrate. When the substrate was continually stored for another month, there is no further transformation of its structure and morphology, which may be caused by the presence of the surface

oxidation layer and the inert storage environment (Figure 8e, f). The corresponding evolution of the SERS spectrum from these aged substrates is illustrated in Figure 8g. It can be seen that the SERS intensity degraded significantly after one-month storing, and then the signal intensity remained within a range of modest variation after an additional month's time. Such a trend is shown more clearly by illustrating the corresponding intensity of the peak at 1078 and 1587 cm^{-1} in Figure 8h, and based on the temporal structural change, it can be inferred that the first decreasing of the intensity may be attributed to the oxidation of the surface Ag NPs, which suppresses their SERS activities, and then the formation of Ag_2O layer hinder the further oxidation of other Ag NPs, thus render the substrate promising stability.[45-46] All in all, the time-dependent experiment displays that the morphology of the samples did not change drastically and the SERS intensity was stable within a certain range, even when the oxidation and aggregation of Ag NPs exist to some extent. In addition, some protective chemical species have been utilized to control the aggregation of Ag NPs and ensure their mechanical stability.[11,47] Nevertheless, the existence of these surface species will hinder their following applications. In future work, we will also try to introduce protective surface molecules during the storage of sample and degrade them under photocatalysis to fully utilize the multifunctional hybrid nanostructure.

3.5 Establishing of Calibration Curve for Recyclable SERS-based Detection

To explore the practical applications of the flower-like MoS_2@Ag hybrid substrate with remarkable photocatalytic and SERS properties in recyclable biochemical detection, two of the most commonly agricultural pesticides TMTD and MP were selected as

model pollutants in this study. As an extensively used fungicide, TMTD can protect agricultural crops from downy mildew, kenaf anthracnose, and yellow spot during the seedling stage.[48-50] While, MP is a prototypical organophosphorus insecticide, which can inhibit the activity of alkali-ester in the nerve of insect pests to kill them.[10,52-54] As shown in Figure 9a, SERS spectrum of TMTD with concentration of 1.0×10^{-1} mg/mL on the hybrid substrate exhibits prominent characteristic peaks at 562, 1145, 1376, and 1508 cm^{-1}, which can be assigned to υ(S-S), ρ(CH_3) or υ(C-N), and ρ(CH_3), respectively.[49] After UV irradiation, all these characteristic peaks of TMTD were completely removed, which can be ascribed to the improved photocatalytic capability of MoS_2 with the help of Ag NPs. When the same substrate after photocatalysis was applied in the second detection of TMTD with diluted concentration, characteristic peaks with decreased intensity can be detected again, indicating the reusability of the substrate. Such detection and photocatalytic process was continually preceded for TMTD by progressively reducing concentration, and it is inspiring to find that the signal of TMTD could be well observed even at 1.0×10^{-6} mg/mL after six cycles of reactions. Then, the correlation between the SERS intensity and the molecule concentration is linearly fitted with R^2 value of 0.991 and illustrated in Figure 9b. The LOD was estimated to be 6.4×10^{-7} mg/mL, which is extremely lower than the minimal residue limit (MRL) of 7 ppm in fruit prescribed by the U.S. Environmental Protection Agency (EPA).[9] Meanwhile, the recyclable detection of MP by using the hybrid substrate was also demonstrated as shown in Figure 9c. The main characteristic peaks at 1112, 1344, and 1588 cm^{-1} can be attributed to C−N stretch, C−O bend, and phenyl stretch,

respectively.[52-53] And R^2 value of 0.986 was obtained (Figure 9d). After a linear fitting of the SERS intensity at 1344 cm^{-1} toward molecule concentration, the LOD for MP was concluded as 9.8×10^{-7} mg/mL. The successful establishing of the calibration curve between the SERS intensity and the concentration of the standard molecule solution readily enable the following assay of pesticide residue on the peels of vegetables and fruits. Meanwhile, the current substrate was also compared with other reported ones for TMTD and MP detection as shown in Table 2. It is found that the LOD achieved here is not the lowest one in comparison with the other results. The possible reason for such vulnerable sensitivity can be probably attributed to the smaller size and less dense of the magnetron sputtering Ag NPs than those prepared by chemical method, which leads to fewer "hot spots". In fact, density and aggregation degree of Ag NPs all play critical roles in obtaining high SERS activity.[54] As discussed above, the enrichment of Ag NPs after extending the sputtering time to 120 and 140 s could indeed increase the SERS activity and improve the detection sensitivity. However, the photocatalytic efficiency of the sample modified with too many Ag NPs is relatively poor. With regard to obtaining both good SERS sensitivity and photocatalytic ability, the MoS_2@Ag substrate synthesized with sputtering time of 100 s was finally chose to enable the following in-situ recyclable multiplexed assay of TMTD and MP on different kinds of fruits and vegetables with various sizes and surface roughnesses, which has not been investigated before to the best of our knowledge. It is also imagined that the detection sensitivity can be improved by tuning the morphology of MoS_2 matrix or modifying Ag

NPs with better size and aggregation status by in-situ reducing strategy, which will be carried out in our next work.

3.6 Simultaneous Recyclable Detection of Multi-Pesticides on Different Vegetables and Fruits

In previous works, most of the fruits and vegetables applied for in-situ SERS-based monitoring are those with large size and few wrinkles on the surface.[2,10,51-52] Whereas, owing to the wide application of pesticide in agriculture, it is of extreme importance to realize the ultra-sensitive assay of pesticide residues on vegetables and fruits with diverse sizes and surface roughnesses to ensure food safety under different conditions. In this regard, a series of foods including eggplant, Chinese cabbage, grape, and strawberry were chose as recyclable detection models by following the rules from relatively big size to small one and from smooth surface to rough one. Figure 10 shows the SERS signals of the target TMTD and MP collected on all these real samples, representing the evidence of the astonishing enhancement ability of the hybrid substrate. More specifically, the first cycle of recyclable SERS-based detection from eggplant, Chinese cabbage, grape, to strawberry is shown in Figure 10a, b. Then, the SERS intensities obtained in the above experiment were subsequently used to fit the calibration curve (Figure 9 b, d), and the recoveries of the calculated data to the real ones are illustrated in Figure 10e, f. It is interesting to find that the recovery presents a drift trend with the decrease of the sample size (eggplant to grape or Chinese cabbage to strawberry), which may due to the fact that the fitting between the rigid SERS-active substrate and the small sample is not as good as that between the substrate and the large

one. In the meanwhile, when the surface of the food becomes rougher (eggplant to Chinese cabbage or grape to strawberry), a significant decline of the recovery was observed as well, which could also be attributed to the difficulty of tightly contacting the SERS-active substrate to the surface of food. Besides, some target molecules even lies into the surface folds and cracks of the food, which further reduce the effective pesticide molecules collected on the substrate. In total, the detection recovery on these foods ranges from 95.5% to 63.1% for TMTD and 92.3% to 62.6% for MP respectively. Although the results for the foods with smaller size and more wrinkles were not so ideal, all the detection recoveries were higher than 60% and different cycle sequences resulted in a deviation of only 8%, which can already reveal the feasibility of the developed hybrid substrate for simple and fast determination of pesticide residues. A flexible Ag/Au NWs/PDMS film developed in our recent work presented advantage over the rigid ones because of their ability to conform to the curved object for the directly efficient extraction of target molecules.[52] Thence, it may be another innovative potential design to combine the MoS_2@Ag nanocomposites with such flexible matrix to further improve their application universality. Moreover, it should be pointed out that the assay of TMTD or MP on different foods was also conducted utilizing only one SERS-active substrate according to the recyclable process combined with detection and photocatalysis. Therefore, the obtained recovery may fluctuate under different recyclable sequence from eggplant to strawberry or the inverse one. Therefore, the measured concentration and the corresponding recoveries under the recyclable sequence from strawberry to eggplant were also collected (Figure 10c, d) and

summarized in Figure 10e, f as second cycle. It can be seen that the fluctuation of these data due to the recyclable sequence limits within 8% (Figure 10f), indicating the reliability and reproducibility of the SERS detection and photocatalysis strategy.

From the view of protecting vegetables and fruits from various diseases and insects, most of the time, two or more mixed pesticide should be used during their growth process. However, this fact can lead to multi-pesticide residues which seriously threaten food safety and ecological protection. Therefore, it is of immense importance to quantitative detecting the mixture of TMTD and MP with different concentration ratios on the foods. As it is known, besides ultra-high sensitivity of even single-molecule level, another unique superior of SERS technology lies in its ultra-narrow spectral line width, which is more beneficial for multiplexed detection compared with other method. Therefore, the SERS-based detection of various mixed molecules have been intensively investigated to promote the practical application of SERS technology.[14,45,53-54] In this work, the solutions of TMTD and MP with the same volume and different concentrations were mixed together and resulted in the mixed solution with various concentration ratios of 8:2, 6:4, 5:5, 4:6, and 2:8. And then, these mixtures were dropped on the surface of eggplant and evaporated before recyclable detection, respectively. From the collected SERS spectra presented in Figure 11a, the characteristic peaks of TMTD and MP, which are marked separately, can both be identified without any interference owing to the ultra-narrow width of the Raman peak. Meanwhile, it is obviously observed from Figure 11b that the characteristic peak intensity of TMTD at 1376 cm^{-1} gradually became stronger with increasing TMTD

concentration, while the characteristic peak intensity of MP at 1344 cm^{-1} progressively reduced along with decreasing MP concentration. It is envisioned that the simultaneous recyclable detection of multi-molecule can be effectively facilitated by the substrate with remarkable SERS and photocatalytic properties. Attributed to the relatively evident SERS peaks of the molecules, the mixed solution of TMTD and MP with concentration ratio of 8:2 was then selected to further test the multicomponent detection ability of the recyclable hybrid substrate on different vegetables and fruits. As illustrated in Figure 11 c, the characteristic peaks of TMTD and MP at 1376 and 1344 cm^{-1} can both be clearly distinguished, which verifies the realization of multicomponent detection on different foods. In addition, attributed to its relatively large and smooth surface, which is good for the binding of target molecule and substrate, the eggplant gave out the strongest SERS signal. While, the SERS signal gradually decreased with the food became smaller and their surface changed to rougher. Such a trend is clearly presented in Figure 11d. These results evidence that the in-situ recyclable detection of two kinds of pesticides on fruits and vegetables was effectively demonstrated, which is promising from a food safety standpoint. However, it can be imagine that too many added pesticide residues or other impurities will interfere with each other due to the overlapping of their characteristic Raman peaks. Even worse, it is a great challenge to distinguish a target molecule with low concentration from numerous colleagues. Therefore, it is of extreme importance to further pave the way for practical multiplex detection such as design and develop other powerful substrates with higher electromagnetic enhancement ability.

4. Conclusions

In summary, an efficient SERS-active MoS_2@Ag hybrid substrate was put forward to realize recyclable detection of pesticide residues. Significant SERS effect and photocatalytic activity were simultaneously observed due to the presence of Ag layer on the flower-like MoS_2 matrix, which could generate enough electromagnetic "hot spots" and act as an electron reservoir to prevent the combination of electron-hole pairs. The MoS_2@Ag hybrid substrate synthesized with sputtering time of 100 s exhibited the highest photocatalytic efficiency and SERS EF of 1.1×10^6, which was then used to recyclable detect TMTD and MP on eggplant, Chinese cabbage, grape, and strawberry, respectively. Gradually declined detection recoveries from 95.5% to 63.1% for TMTD and 92.3% to 62.6% for MP verified the difficulty of in-situ monitoring of molecules on the small foods with rough surfaces and the adaptation of the developed substrate. Importantly, trace mixed residues with different concentration ratios on these fruits and vegetables could be simultaneously detected by the MoS_2@Ag hybrid substrate, demonstrating its great potential in practical on-site monitoring and analysis of multicomponent pesticide residues.

ASSOCIATED CONTENT

Supporting Information

The Supporting Information is available free of charge via the Internet at http://pubs.acs.org.

AUTHOR INFORMATION

Corresponding Author

E-mail: jiangtao@nbu.edu.cn (T.J.) and guchenjie@nbu.edu.cn (C.G.)

Notes

The authors declare no competing financial interest.

ACKNOWLEDGMENT

This work was supported by National Natural Science Foundation of China (Grant No. 61675104), Natural Science Foundation of Zhejiang Province (Grant No. LY19F050002), the Natural Science Foundation of Ningbo (Grant No. 2018A610316), K.C. Wong Magna Fund in Ningbo University, China, Applied Basic Research Project of Shanxi Province (Grant No. 201701D221096), and Science and Technology Innovation Project of University of Shanxi Province (Grant No.2019L0746).

REFERENCES

(1) Larsen, A. E.; Gaines, S. D.; Deschênes, O. Agricultural Pesticide Use and Adverse Birth Outcomes in The San Joaquin Valley of California. *Nat. Commun.* **2017**, *8* (1), 302.

(2) Zhang, Y.; Wang, Z.; Wu, L.; Pei, Y.; Chen, P.; Cui, Y. Rapid Simultaneous Detection of Multi-Pesticide Residues on Apple Using SERS Technique. *Analyst* **2014**, *139* (20), 5148-5154.

(3) Pano-Farias, N. S.; Ceballos-Magaña, S. G.; Muñiz-Valencia, R.; Jurado, J. M.; Alcázar, Á.; Aguayo-Villarreal, I. A. Direct Immersion Single Drop Micro-Extraction Method for Multi-class Pesticides Analysis in Mango Using GC-MS. *Food. Chem.* **2017**, *237*, 30-38.

(4) Lavagnini, I.; Urbani, A.; Magno, F. Overall Calibration Procedure via A Statistically Based Matrix-Comprehensive Approach in The Stir Bar Sorptive Extraction–Thermal Desorption-Gas Chromatography–Mass Spectrometry Analysis of Pesticide Residues in Fruit-Based Soft Drinks. *Talanta*

2011, *83* (5), 1754-1762.

(5) Tuzimski, T.; Rejczak, T. Application of HPLC–DAD After SPE/QuEChERS with ZrO_2-Based Sorbent in D-SPE Clean-up Step for Pesticide Analysis in Edible Oils. *Food. Chem.* **2016**, *190*, 71-79.

(6) Peres, G. T.; Rath, S.; Reyes, F. G. R. A HPLC with Fluorescence Detection Method for The Determination of Tetracyclines Residues and Evaluation of Their Stability in Honey. *Food. Control.* **2010**, *21* (5), 620-625.

(7) Lan, M.; Guo, Y.; Zhao, Y.; Liu, Y.; Gui, W.; Zhu, G. Multi-Residue Detection of Pesticides Using A Sensitive Immunochip Assay Based on Nanogold Enhancement. *Anal. Chim. Acta*. **2016**, *938*, 146-155.

(8) Haynes, C. L.; McFarland, A. D.; Van Duyne, R. P. Surface-Enhanced Raman Spectroscopy. *Anal. Chem.* **2005**, 77, *17*, 338 A-346 A.

(9) Yuan, C.; Liu, R.; Wang, S.; Han, G.; Han, M. Y.; Jiang, C.; Zhang, Z. Single Clusters of Self-Assembled Silver Nanoparticles for Surface-Enhanced Raman Scattering Sensing of A Dithiocarbamate Fungicide. *J. Mater. Chem.* **2016**, *21* (40), 16264-16270.

(10) Jiang, T.; Wang, X.; Tang, J.; Tang, S. Seed-Mediated Synthesis of Floriated Ag Nanoplates as Surface Enhanced Raman Scattering Substrate for In Situ Molecular Detection. *Mater. Res. Bul*. **2018**, *97*, 201-206.

(11) Cao, Y.; Zhang, J.; Yang, Y.; Huang, Z.; Long, N. V.; Fu, C. Engineering of SERS Substrates Based on Noble Metal Nanomaterials for Chemical and Biomedical Applications. *Appl. Spectrosc. Rev.* **2015**, *50* (6), 499-525.

(12) McCann, M. T.; Mooney, D. A.; Rahman, M.; Dowling, D. P.; MacElroy, J. D. Novel, Nanoporous Silica and Titania Layers Fabricated by Magnetron Sputtering. *ACS Appl. Mater. Inter.* **2011**, *3* (2), 252-260.

(13) Sinha, G.; Depero, L. E.; Alessandri, I. Recyclable SERS Substrates Based on Au-coated ZnO Nanorods. *ACS Appl. Mater. Inter.* **2011**, *3* (7), 2557-2563.3

(14) Fang, H.; Zhang, C. X.; Liu, L.; Zhao, Y. M.; Xu, H. J. Recyclable Three-Dimensional Ag Nanoparticle-Decorated TiO_2 Nanorod Arrays for Surface-Enhanced Raman Scattering. *Biosens. Bioelectron.* **2015**, *64*, 434-441.

(15) Alessandri, I.; Lombardi, J. R. Enhanced Raman Scattering with Dielectrics. *Chem. Rev.* **2016**, *116* (24), 14921-14981.

(16) Su, S.; Zhang, C.; Yuwen, L.; Chao, J.; Zuo, X.; Liu, X.; Song, C.; Fan, C.; Wang, L. Creating SERS Hot Spots on MoS_2 Nanosheets with In Situ Grown Gold Nanoparticles. *ACS Appl. Mater. Inter.* **2014**, *6* (21), 18735-18741.

(17) Zhao, Y.; Deng, G.; Liu, X.; Sun, L.; Li, H.; Cheng, Q.; Xi, K.; Xu, D. MoS_2/Ag Nanohybrid: A Novel Matrix with Synergistic Effect for Small Molecule Drugs Analysis by Negative-Ion Matrix-Assisted Laser Desorption/Ionization Time-of-Flight Mass Spectrometry. *Anal. Chim. Acta.* **2016**, *937*, 87-95.

(18) Zuo, P.; Jiang, L.; Li, X.; Li, B.; Ran, P.; Li, X.; Qu, L.; Lu, Y. Metal (Ag, Pt) -MoS_2 Hybrids Greenly Prepared Through Photochemical Reduction of Femtosecond Laser Pulses for SERS and HER. *ACS Sustain. Chem. Eng.* **2018**, *6* (6), 7704-7714.

(19) Cheah, A.; Chiu, W.; Khiew, P.; Nakajima, H.; Saisopa, T.; Songsiriritthigul, P.; Radiman, S.; Hamid, M. A. A. Facile Synthesis of A Ag/MoS_2 Nanocomposite Photocatalyst for Enhanced Visible-Light Driven Hydrogen Gas Evolution. *Catal. Sci. Technol.* **2015**, *5* (8), 4133-4143.

(20) Yang, L.; Zhong, D.; Zhang, J.; Yan, Z.; Ge, S.; Du, P.; Jiang, J.; Sun, D.; Wu, X.; Fan, Z. Optical Properties of Metal–Molybdenum Disulfide Hybrid Nanosheets and Their Application for Enhanced

Photocatalytic Hydrogen Evolution. *ACS Nano* **2014**, *8* (7), 6979-6985.

(21) Liang, X.; Wang, Y. S.; You, T. T.; Zhang, X. J.; Yang, N.; Wang, G. S.; Yin, P. G. Interfacial Synthesis of A Three-Dimensional Hierarchical MoS_2-NS@Ag-NP Nanocomposite as A SERS Nanosensor for Ultrasensitive Thiram Detection. *Nanoscale* **2017**, *9* (25), 8879-8888.

(22) Singha, S. S.; Mondal, S.; Bhattacharya, T. S.; Das, L.; Sen, K.; Satpati, B.; Das, K.; Singha, A. Au Nanoparticles Functionalized 3D-MoS_2 Nanoflower: An Efficient SERS Matrix for Biomolecule Sensing. *Biosens. Bioelectron.* **2018**, *119*, 10-17.

(23) Zhang, H.; Zhang, W.; Gao, X.; Man, P.; Sun, Y.; Liu, C.; Li, Z.; Xu, Y.; Man, B.; Yang, C. Formation of The AuNPs/GO@MoS_2/AuNPs Nanostructures for The SERS Application. *Sensors. Actuat. B-Chem.* **2019**, *282*, 809-817.

(24) Lin, H.; Chen, X.; Li, H.; Yang, M.; Qi, Y. Hydrothermal Synthesis and Characterization of MoS_2 Nanorods. *Mate. Lett.* **2010**, *64* (15), 1748-1750.

(25) Zheng, X.; Xu, J.; Yan, K.; Wang, H.; Wang, Z.; Yang, S. Space-Confined Growth of MoS_2 Nanosheets within Graphite: The Layered Hybrid of MoS_2 and Graphene as An Active Catalyst for Hydrogen Evolution Reaction. *Chem. Mater.* **2014**, *26* (7), 2344-2353.

(26) Bai, Y. L.; Liu, Y. S.; Ma, C.; Wang, K. X.; Chen, J. S. Neuron-Inspired Design of High-Performance Electrode Materials for Sodium-Ion Batteries. *ACS Nano* **2018**, *12* (11), 11503-11510.

(27) Zhang, X.; Yu, Z.; Ji, W.; Sui, H.; Cong, Q.; Wang, X.; Zhao, B. Charge-Transfer Effect on Surface-Enhanced Raman Scattering (SERS) in An Ordered Ag NPs/4-Mercaptobenzoic Acid/TiO_2 System. *J. Phys. Chem. C.* **2015**, *119* (39), 22439-22444.

(28) Wang, C.; Wang, J.; Li, P.; Rong, Z.; Jia, X.; Ma, Q.; Xiao, R.; Wang, S. Sonochemical Synthesis of Highly Branched Flower-Like Fe_3O_4@SiO_2@Ag Microcomposites and Their Application as Versatile

SERS Substrates. *Nanoscale* **2016**, *8* (47), 19816-19828.

(29) Yüksel, S.; Ziegler, M.; Goerke, S.; Huebner, U.; Weber, K.; Schaaf, P.; Meyer, H. G.; Cialla-May, D.; Popp, J. R. Hierarchically-Designed 3D Flower-Like Composite Nanostructures as An Ultrastable, Reproducible, and Sensitive SERS Substrate. *ACS Appl. Mater. Inter.* **2017**, *9* (44), 38854-38862.

(30) Lu, P.; Lang, J.; Weng, Z.; Rahimi-Iman, A.; Wu, H. Hybrid Structure of 2D Layered GaTe with Au Nanoparticles for Ultrasensitive Detection of Aromatic Molecules. *ACS Appl. Mater. Inter.* **2018**, *10* (1), 1356-1362.

(31) Wu, D.; Chen, J.; Ruan, Y.; Sun, K.; Zhang, K.; Xie, W.; Xie, F.; Zhao, X.; Wang, X. A Novel Sensitive and Stable Surface Enhanced Raman Scattering Substrate Based on A MoS_2 Quantum Dot/Reduced Graphene Oxide Hybrid System. *J. Mater. Chem. C.* **2018**, *6* (46), 12547-12554.

(32) Wang, Z.; Yang, H.; Wang, M.; Petti, L.; Jiang, T.; Jia, Z.; Xie, S.; Zhou, J. SERS-Based Multiplex Immunoassay of Tumor Markers Using Double SiO_2@Ag Immune Probes and Gold-Film Hemisphere Array Immune Substrate. *Colloid. Surface. A* **2018**, *546*, 48-58.

(33) Alessandri, I. Enhancing Raman Scattering without Plasmons: Unprecedented Sensitivity Achieved by TiO_2 Shell-Based Resonators. *J. Am. Chem. Soc.* **2013**, *135* (15), 5541-5544.

(34) Lai, H.; Ma, G.; Shang, W.; Chen, D.; Yun, Y.; Peng, X.; Xu, F. Multifunctional Magnetic Sphere-MoS_2@Au Hybrid for Surface-Enhanced Raman Scattering Detection and Visible Light Photo-Fenton Degradation of Aromatic Dyes. *Chemosphere* **2019**, *223*, 465-473.

(35) Zhang, Y.; Yu, X.; Jia, Y.; Jin, Z.; Liu, J.; Huang, X. A Facile Approach for The Synthesis of Ag-Coated Fe_3O_4@TiO_2 Core/Shell Microspheres as Highly Efficient and Recyclable Photocatalysts. *Eur. J. Inorg. Chem*. **2011**, *2011*(33), 5096-5104.

(36) Xie, Y.; Meng, Y. SERS Performance of Graphene Oxide Decorated Silver Nanoparticle/Titania

Nanotube Array. *RSC Adv.* **2014**, *4* (79), 41734-41743.

(37) Ma, L.; Wu, H.; Huang, Y.; Zou, S.; Li, J.; Zhang, Z. High-Performance Real-Time SERS Detection with Recyclable Ag Nanorods@HfO_2 Substrates. *ACS Appl. Mater. Inter.* **2016**, *8* (40), 27162-27168.

(38) Huang, J.; Ma, D.; Chen, F.; Chen, D.; Bai, M.; Xu, K.; Zhao, Y. Green In Situ Synthesis of Clean 3D Chestnutlike Ag/WO_{3-x} Nanostructures for Highly Efficient, Recyclable and Sensitive SERS Sensing. *ACS Appl. Mater. Inter.* **2017**, *9* (8), 7436-7446.

(39) Ma, Y.; Yang, L.; Yang, Y.; Peng, Y.; Wei, Y.; Huang, Z. Multifunctional Ag-Decorated g-C_3N_4 Nanosheets as Recyclable SERS Substrates for CV and RhB Detection. *RSC Adv.* **2018**, *8* (39), 22095-22102.

(40) Michaelson, H. B. The Work Function of The Elements and Its Periodicity. *J. Appl. Phys.* **1977**, *48* (11), 4729-4733.

(41) McDonnell, S.; Addou, R.; Buie, C.; Wallace, R. M.; Hinkle, C. L. Defect-Dominated Doping and Contact Resistance in MoS_2. *ACS Nano* **2014**, *8* (3), 2880-2888.

(42) Tan, T. T. Y.; Yip, C. K.; Beydoun, D.; Amal, R. Effects of Nano-Ag Particles Loading on TiO_2 Photocatalytic Reduction of Selenate Ions. *Chem. Eng. J.* **2003**, *95* (1-3), 179-186.

(43) Dong, H.; Zeng, G.; Tang, L.; Fan, C.; Zhang, C.; He, X.; He, Y. An Overview on Limitations of TiO_2-Based Particles for Photocatalytic Degradation of Organic Pollutants and The Corresponding Countermeasures. *Water. Res.* **2015**, *79*, 128-146.

(44) Shrivastava, A.; Gupta, V. B. Methods for the Determination of Limit of Detection and Limit of Quantitation of The Analytical Methods. *Chron. Young Sci.* **2011**, *2* (1), 21.

(45) Wang, P.; Wu, L.; Lu, Z.; Li, Q.; Yin, W.; Ding, F.; Han, H. Gecko-Inspired Nanotentacle Surface-Enhanced Raman Spectroscopy Substrate for Sampling and Reliable Detection of Pesticide Residues in

Fruits and Vegetables. *Anal. Chem.* **2017**, *89* (4), 2424-2431.

(46) Zhu, Y.; Li, M.; Yu, D.; Yang, L. A Novel Paper Rag as 'D-SERS' Substrate for Detection of Pesticide Residues at Various Peels. *Talanta* **2014**, *128*, 117-124.

(47) Vassalini, I.; Rotunno, E.; Lazzarini, L.; Alessandri, I. "Stainless" Gold Nanorods: Preserving Shape, Optical Properties, and SERS Activity in Oxidative Environment. *ACS Appl. Mater. Inter.* **2015**, *7* (33), 18794-18802.

(48) Zhang, C. H.; Zhu, J.; Li, J. J.; Zhao, J. W. Small and Sharp Triangular Silver Nanoplates Synthesized Utilizing Tiny Triangular Nuclei and Their Excellent SERS Activity for Selective Detection of Thiram Residue in Soil. *ACS Appl. Mater. Inter.* **2017**, *9* (20), 17387-17398.

(49) Sun, H.; Liu, H.; Wu, Y. A Green, Reusable SERS Film with High Sensitivity for In-Situ Detection of Thiram in Apple Juice. *Appl. Surf. Sci.* **2017**, *416*, 704-709.

(50) Wu, P.; Zhong, L. B.; Liu, Q.; Zhou, X.; Zheng, Y. M. Polymer Induced One-Step Interfacial Self-Assembly Method for The Fabrication of Flexible, Robust and Free-Standing SERS Substrates for Rapid On-Site Detection of Pesticide Residues. *Nanoscale* **2019**, 11, 12829-12836.

(51) Wu, H.; Luo, Y.; Hou, C.; Huo, D.; Zhou, Y.; Zou, S.; Zhao, J.; Lei, Y. Flexible Bipyramid-AuNPs Based SERS Tape Sensing Strategy for Detecting Methyl Parathion on Vegetable and Fruit Surface. *Sensors. Actuat. B-Chem.* **2019**, *285*, 123-128.

(52) Ma, Y.; Du, Y.; Chen, Y.; Gu, C.; Jiang, T.; Wei, G.; Zhou, J. Intrinsic Raman Signal of Polymer Matrix Induced Quantitative Multiphase SERS Analysis Based on Stretched PDMS Film with Anchored Ag Nanoparticles/Au Nanowires. *Chem. Eng. J.* **2020**, *381*, 122710.

(53) Zhou, N.; Meng, G.; Huang, Z.; Ke, Y.; Zhou, Q.; Hu, X. A flexible Transparent Ag-NC@PE Film as A Cut-and-Paste SERS Substrate for Rapid In Situ Detection of Organic Pollutants. *Analyst* **2016**, *141*

(20), 5864-5869.

(54) Li, C.; Xu, S.; Yu, J.; Jiang, S.; Liu, A.; Li, Z.; Zhang, S.; Zhao, X.; Zhang, C.; Man, B. 3D Hybrid MoS_2/AgNPs/Inverted Pyramid PMMA Resonant Cavity System for The Excellent Flexible Surface Enhanced Raman Scattering Sensor. *Sensors. Actuat. B-Chem.* **2018**, 274, 152-162.

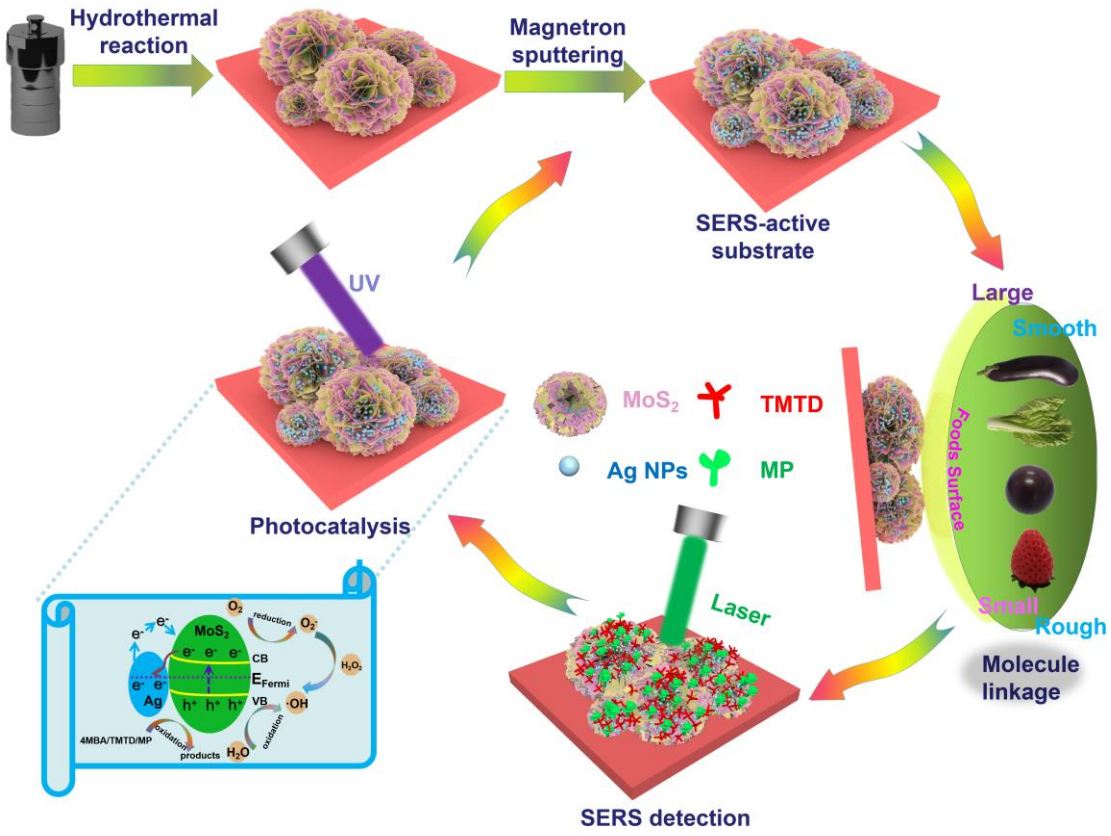

Scheme 1. The typical fabrication process of the flower-like MoS_2@Ag hybird matrix and their application in recyclable monitoring of pesticide residues.

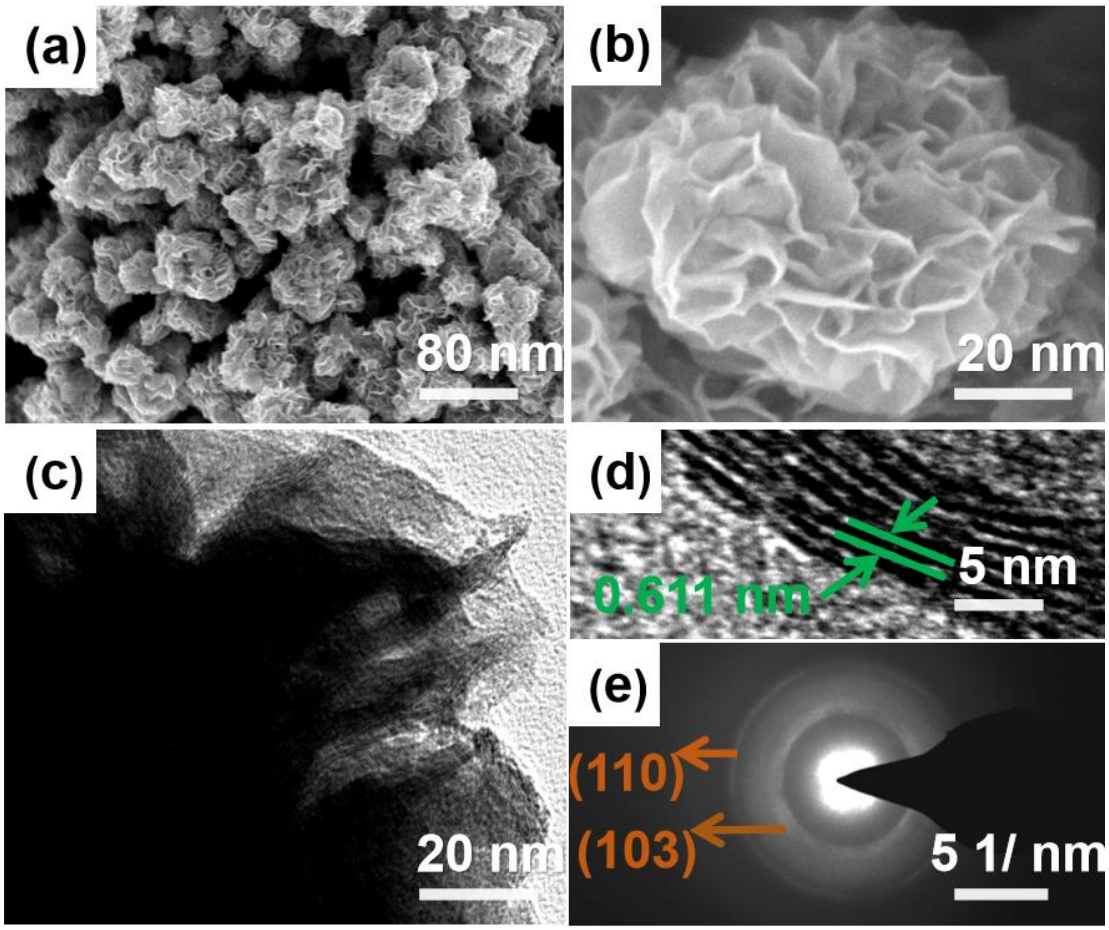

Figure 1. (a, b) SEM, (c) TEM, (d) HRTEM and (e) SAED images of flower-like MoS_2 matrix.

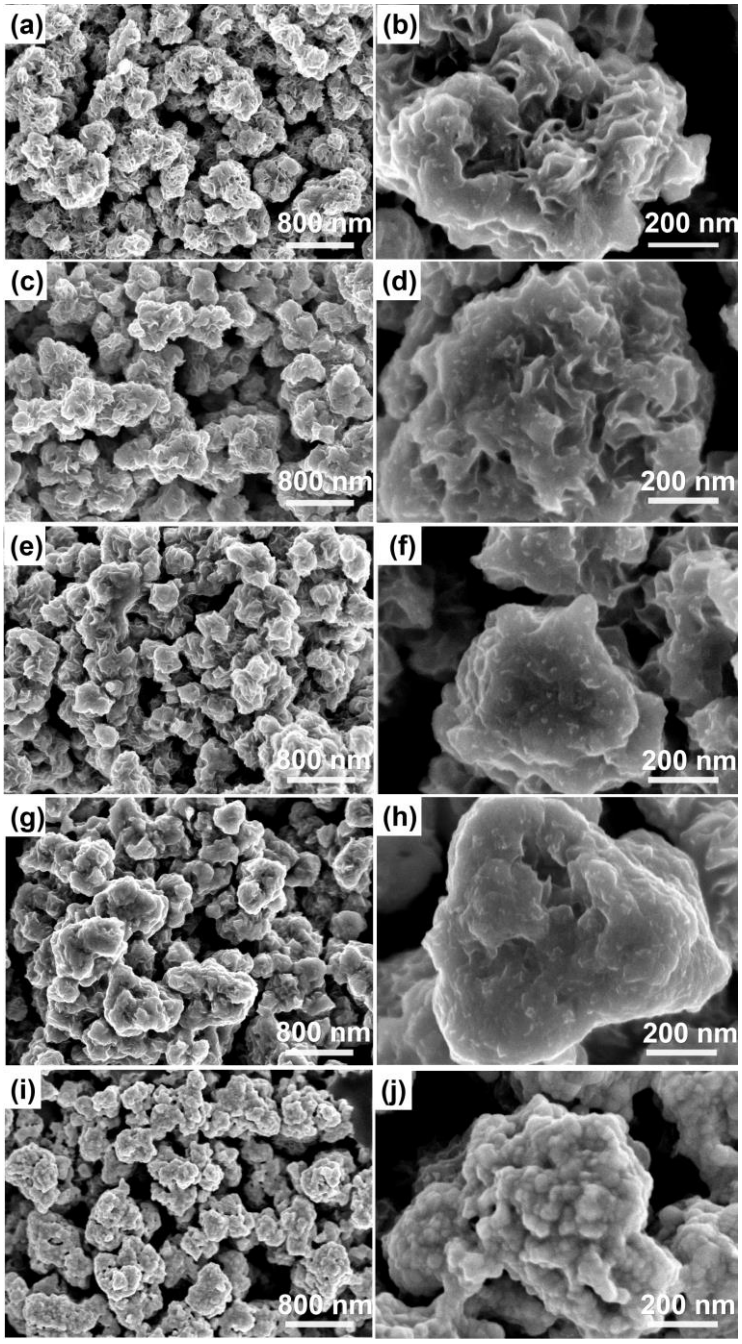

Figure 2. SEM images of flower-like MoS_2@Ag substrates with different sputtering times of (a, b) 60, (c, d) 80, (e, f) 100, (g, h) 120, and (i, j) 140 s, respectively.

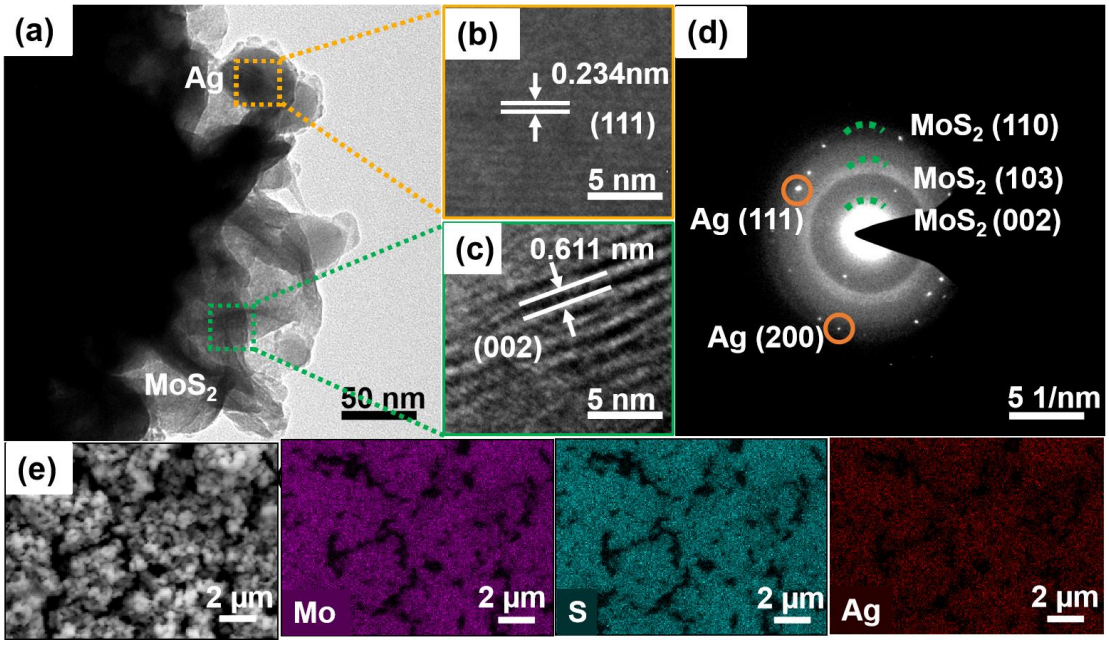

Figure 3. (a) TEM image, (b, c) HRTEM image, (d) SAED pattern, and (e) EDX elemental mapping of Mo, S, and Ag of the flower-like MoS_2@Ag hybrid substrate synthesized with sputtering time of 100 s.

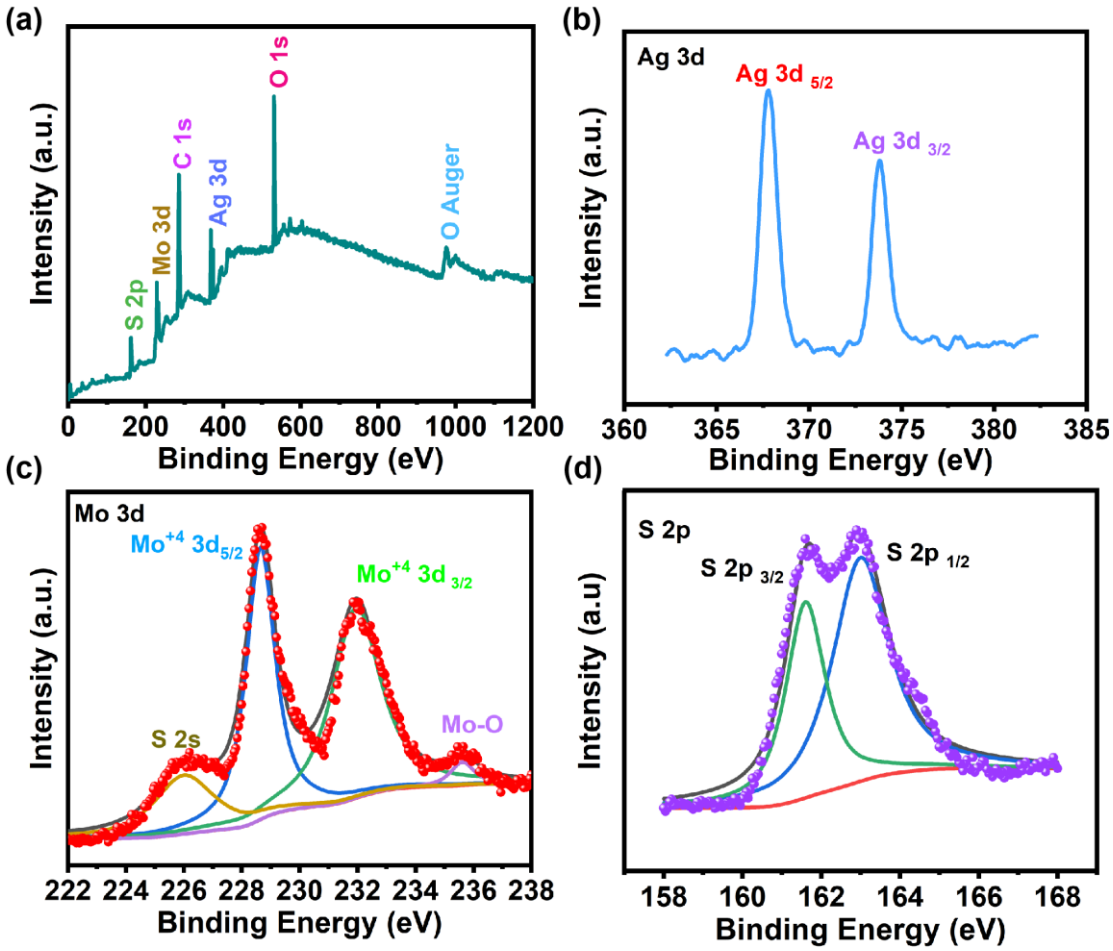

Figure 4. (a) XPS spectrum of the flower-like MoS_2@Ag hybrid substrate synthesized with sputtering time of 100 s, and the corresponding high-resolution spectra of (b) Ag 3d, (c) Mo 3d, and (d) S 2p.

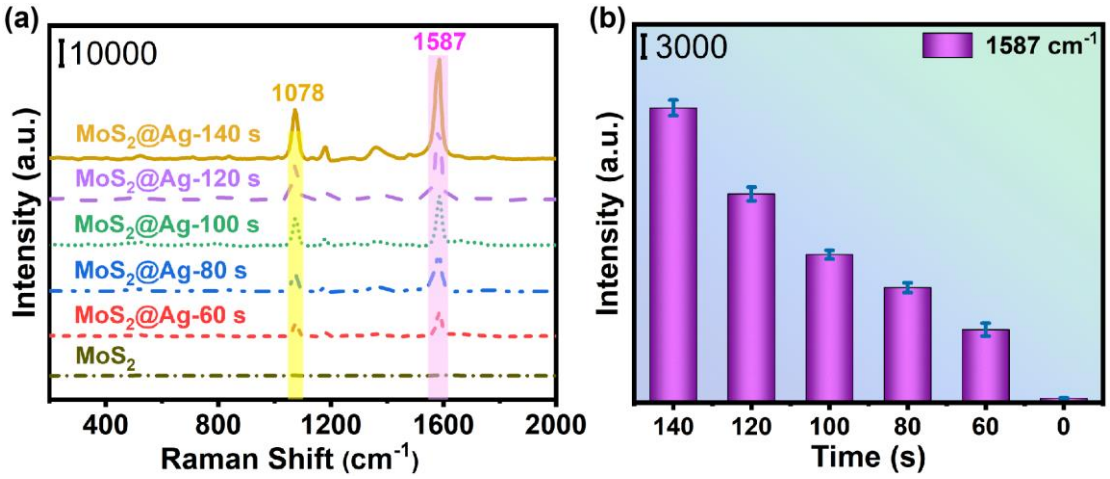

Figure 5. (a) SERS spectra of 4MBA (10 mM) on the pure flower-like MoS_2 matrix and the flower-like MoS_2@Ag hybrid substrates synthesized with sputtering times of 60, 80, 100, 120, and 140 s. (b) Comparison of average Raman intensity of the peak at 1587 cm^{-1}.

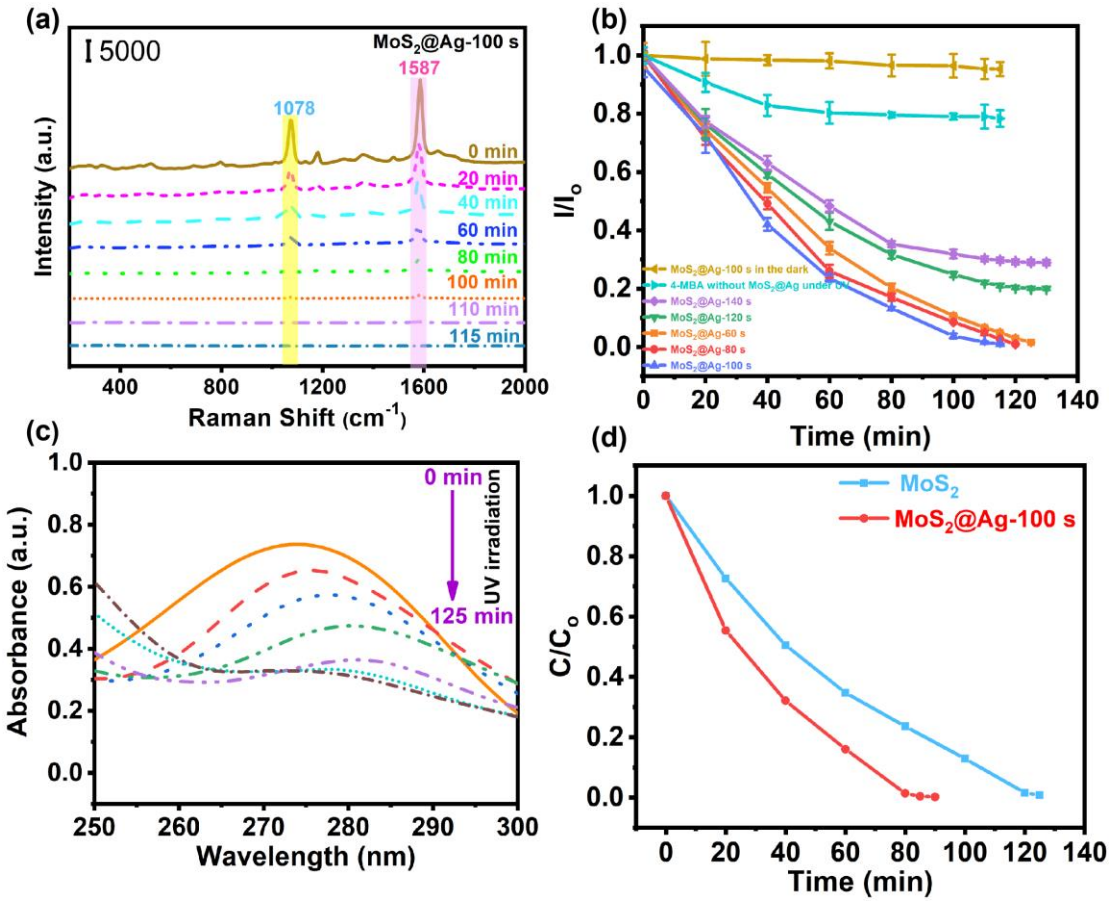

Figure 6. (a) SERS spectra of 4MBA (10 mM) adsorbed on MoS_2@Ag hybrid substrate synthesized with sputtering time of 100 s for different UV irradiation time. (b) The time-dependent ratios of I/I_0 from SERS peak at 1587 cm^{-1} on various MoS_2@Ag hybrid substrates with and without UV irradiation. (c) UV-vis absorption spectra of 4MBA (1 mM) on the substrate of MoS_2 under UV irradiation. (d) The time-dependent ratios of C/C_0 from the absorption spectra of the MoS_2 matrix and MoS_2@Ag hybrid substrate synthesized with sputtering time of 100 s under UV irradiation.

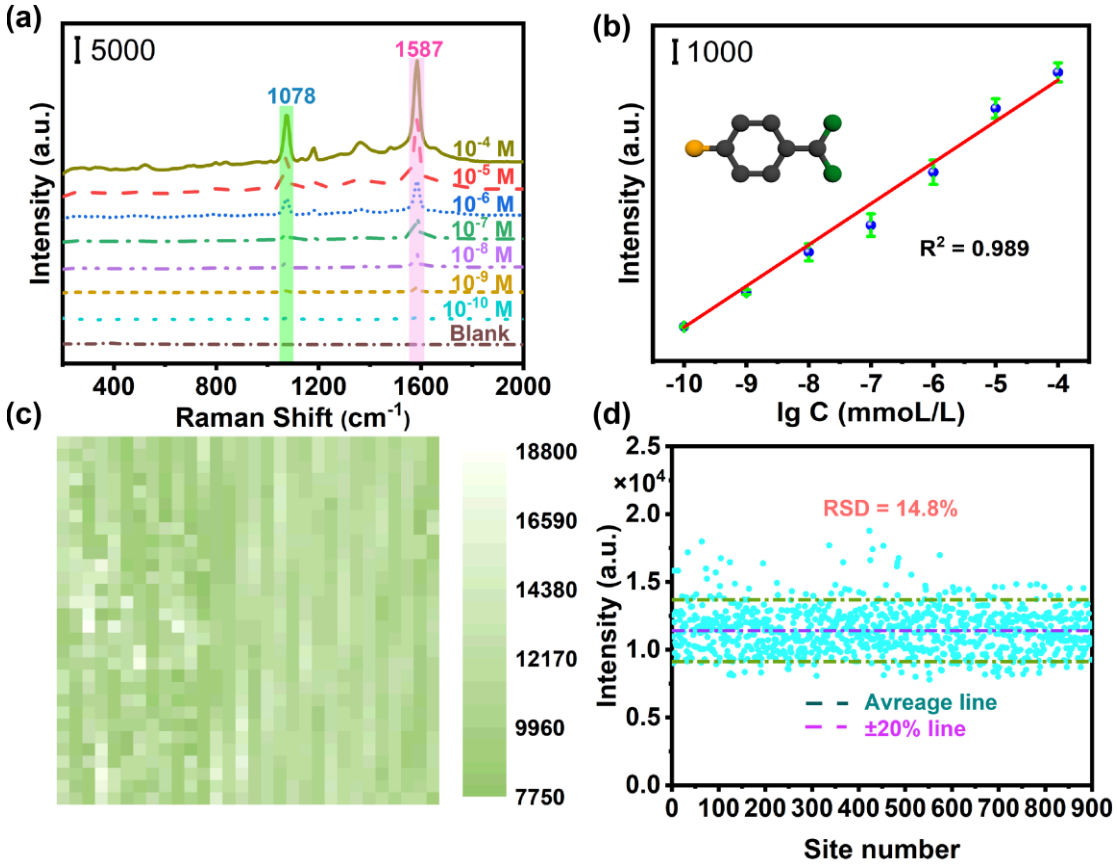

Figure 7. (a) The SERS spectra of 4MBA with the concentration from 10^{-4} to 10^{-10} M on flower-like MoS_2@Ag hybrid substrate and Raman spectrum of blank substrate. (b) The plot of SERS intensities at 1587 cm^{-1} as a function of the logarithm of 4MBA concentration. (c) SERS mapping (600 × 600 μm^2, step size of 20 μm) of the peak at 1587 cm^{-1} recorded from the flower-like MoS_2@Ag hybrid substrate modified with 10^{-4} M 4MBA. (d) The corresponding intensity distribution of all 900 points.

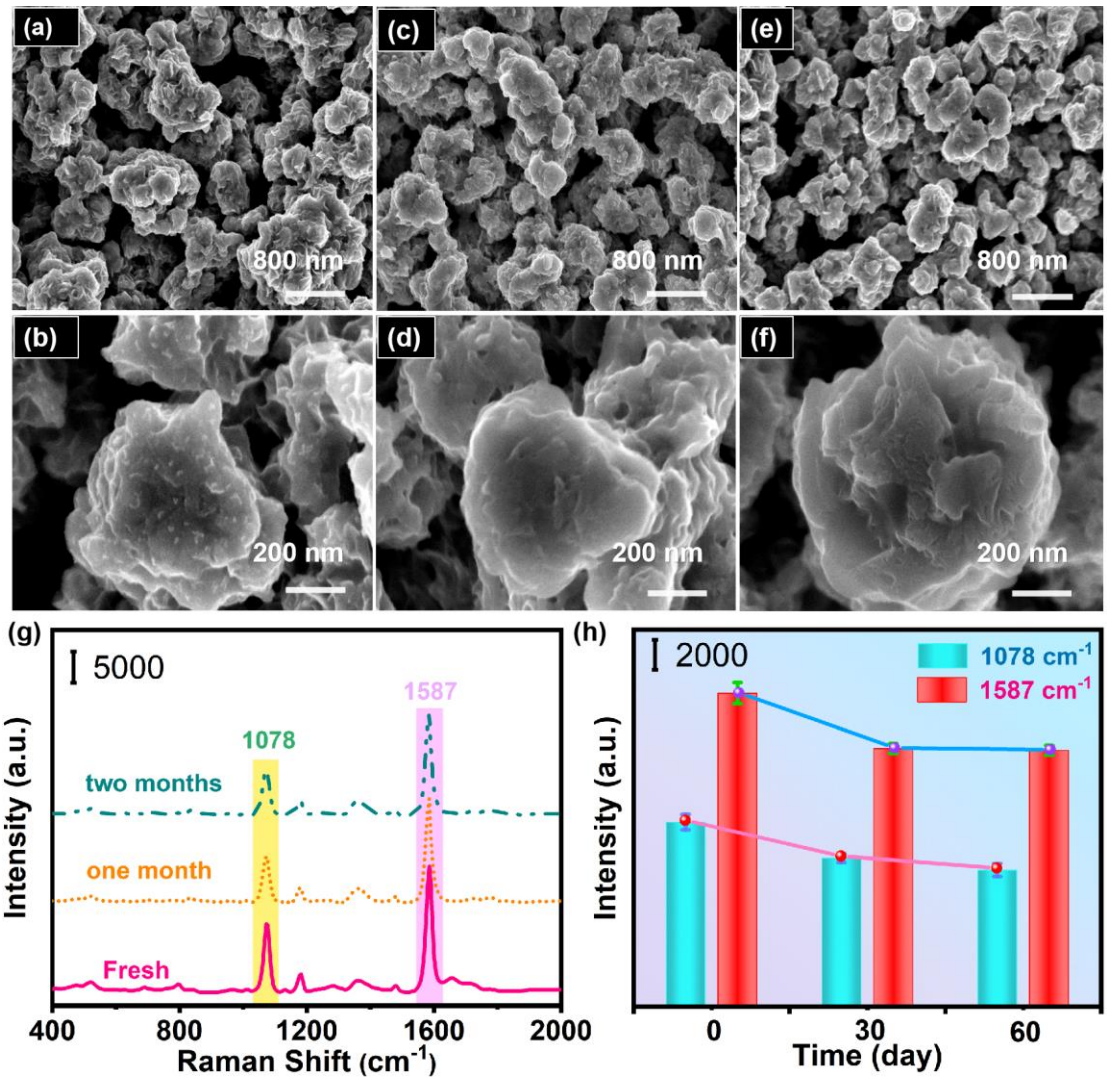

Figure 8. SEM images of flower-like MoS_2@Ag hybrid substrate: (a, b) the fresh one (c, d) stored in air atmosphere for one month, (e, f) stored in air atmosphere for two months. (g) Average SERS spectra of 4MBA (10 mM) on these substrates. (h) The corresponding intensity of the peak at 1078 and 1587 cm^{-1} from these substrates.

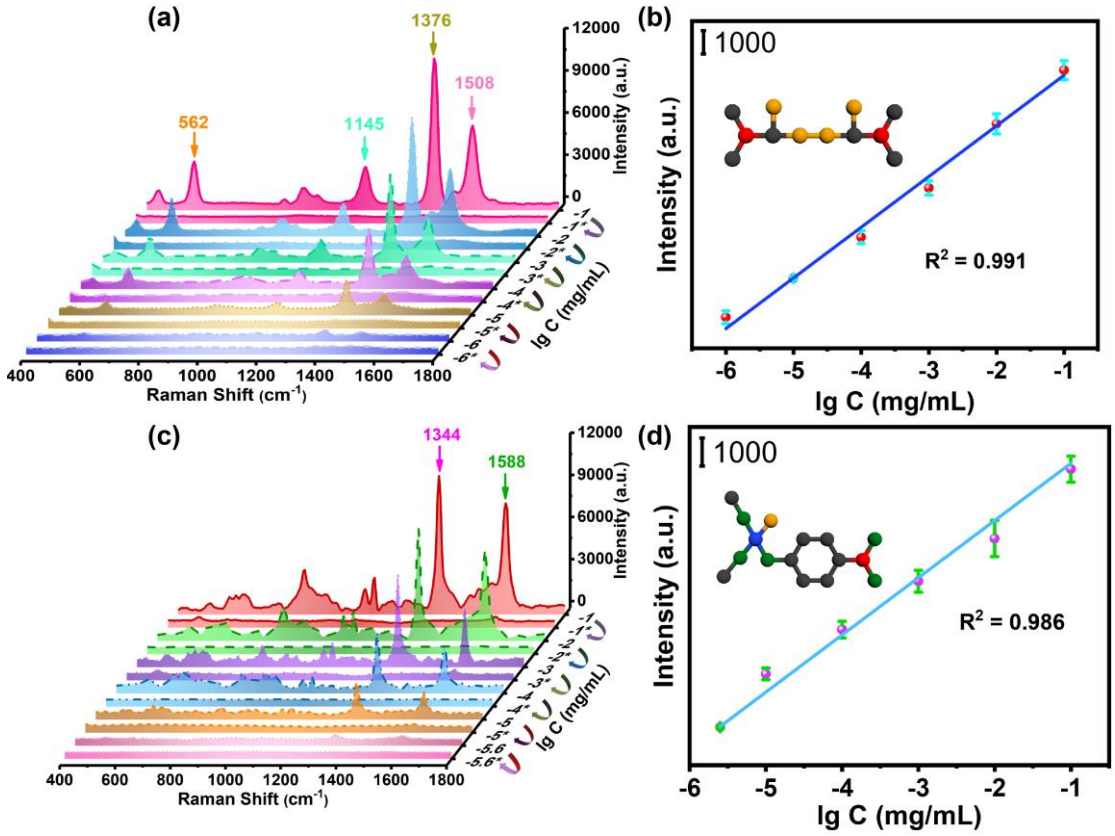

Figure 9. Recycle detection of (a) TMTD and (c) MP at different concentrations based on SERS spectra. The corresponding dose-response curves of (b) the peak intensity at 1376 cm^{-1} for TMTD and (d) the peak intensity at 1344 cm^{-1} for MP.

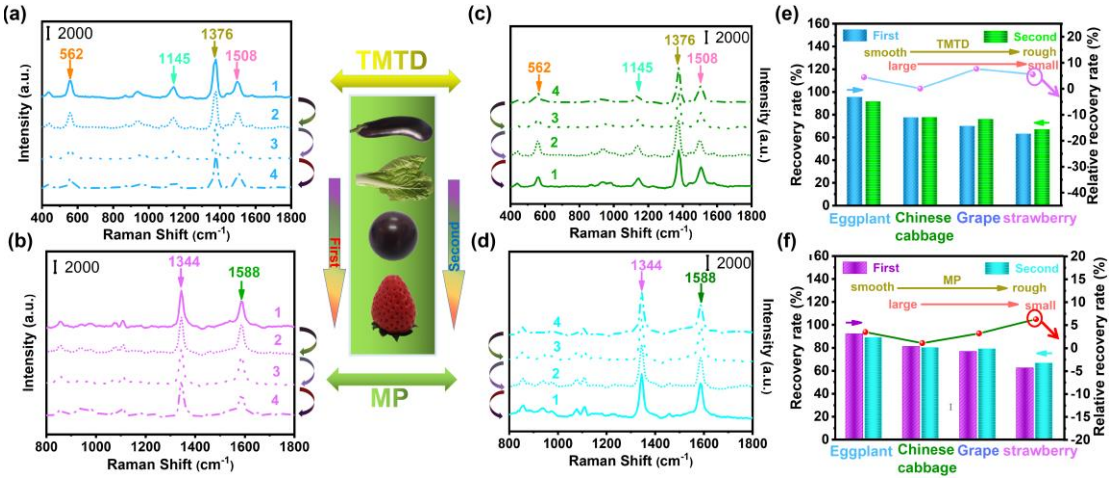

Figure 10. Recyclable SERS-based detection on eggplant (denoted as 1), Chinese cabbage (2), grape (3), and strawberry (4): first cycle for (a) TMTD and (b) MP, second cycle for (c) TMTD and (d) MP. The corresponding recovery rates for the detection of (e) TMTD and (f) MP.

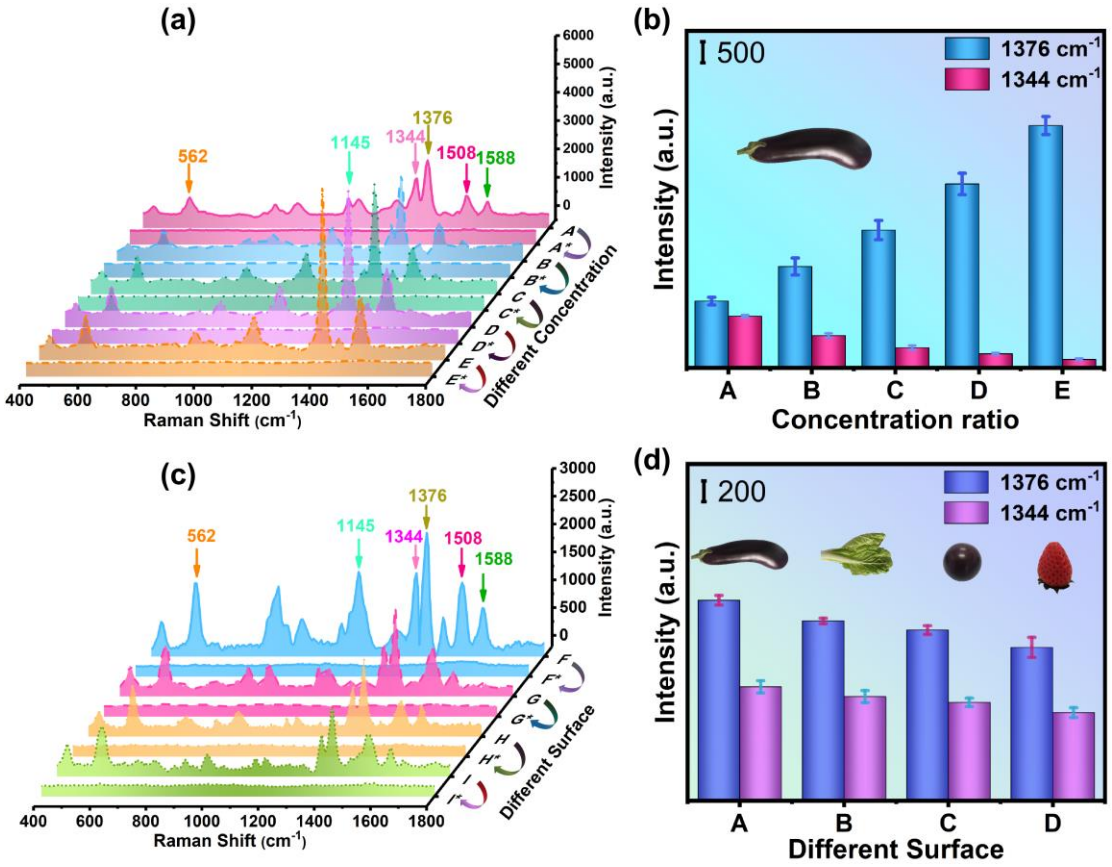

Figure 11. (a) Recyclable SERS-based detection of mixed MP and TMTD with different concentration ratios of A 8:2, B 6:4, C 5:5, D 4:6, and E 2:8 on eggplant. (c) Recyclable SERS-based detection of mixed MP and TMTD with the same concentration on F eggplant, G Chinese cabbage, H grape, and I strawberry. (b, d) The histogram of average SERS intensity of the peak at 1376 and 1344 cm^{-1} according to (a, c).

Table 1 Summary of typical recyclable SERS substrates composed of different semiconductor and plasmonic NPs.

Substrate	The mechanism of charge separations	Targets and LOD	Ref.
Au-ZnO nanorods	Au-semiconductor interface allows for an efficient separation of charges.	Methylene blue; 10^{-12} M	13
Ag-coated Fe_3O_4@TiO_2 microspheres	Ag nanoparticles act as electron scavengers and can effectively suppress the electron-hole recombination.	Methylene blue; -	35
TiO_2-based spherical resonator	UV light induces the formation of e-/h+ pairs in anatase TiO_2 supported by ozone.	Methylene blue; -	33
GO/Ag/TiO_2 nanotube array (NTA)	1. The photogenerated electrons facilely transfer from the conduction band of TiO_2 NTA to Ag NPs through Schottky barriers. 2. Both Ag NPs and GO serve as acceptors of the photogenerated electrons from TiO_2 NTA.	Methylene blue and bisphenol A; 10^{-9} and 5 $\times 10^{-7}$ M	36
Ag nanoparticle-decorated TiO_2 nanorod arrays	1. Deposited Ag NPs would act as traps to capture photo-induced electrons and holes. 2. The plasmon-induced photoexcited electrons can move into the conduction band of TiO_2.	Rhodamine 6G; 10^{-7} M	14

Ag nanorods@HfO_2 shell	The thermal release of adsorbed molecules and regeneration of substrate through annealing.	Methylene blue and crystal violet; -	37
3D chestnut-like Ag/WO_{3-x} nanostructures	The high electron conductivity of the Ag NPs helps to improve the photogenerated electron/hole separation.	Malachite green and thiram; 0.29 pM and 0.32 nM	38
Ag-decorated g-C_3N_4 nanosheets	The photo-excited electrons could transfer from g-C_3N_4 to the surface of the Ag NPs through a quasi-fermi level after their contact.	Crystal violet and rhodamine B; -	39
Magnetic sphere-MoS_2@Au hybrid	1. H_2O_2 as an electron acceptor was added to suppress the fast electron-hole recombination. 2. Under light irradiation, the surface plasmon resonance of AuNPs could generate hot-electrons, which were transferred to MoS_2. 3. Decoration of AuNPs also enhanced the adsorption to visible light.	Crystal violet, malachite green, and methylene blue; 1 pM, 0.15 nM, and 1 nM	34
MoS_2@Ag hybrid nanoflower	The transfer of electrons from the conduction band of MoS_2 to Ag due to the formation of Schottky barrier and the trapping of excited electrons in Ag could effectively accelerate charge separation and prevent the combination of electron-hole pairs.	4-mercaptobenzoic acid, thiram, and methyl parathion; 10^{-10} M, 6.4×10^{-7} and 9.8×10^{-7} mg/mL	This work

Note: Symbol "-" denotes no data of LOD.

Table 2 Summary of detection pesticides, substrates, and LOD.

Pesticides	Substrate	LOD	Ref.
TMTD	Triangular silver nanoplates	90 ng/g	48
TMTD	PMMA/Ag NPs/graphene	0.24 ppm	49
TMTD	AuNPs/PVC film	10 ng/cm^2	50
MP	Floriated Ag nanoplates	1 μg/mL	10
MP	Bipyramid gold NPs	31.6 ng/cm^2	51
MP	Ag/Au NWs/PDMS film	10^{-6} and 10^{-5} mg/mL	52
TMTD and MP	Ag-NC@PE composite film	10 nM	53
TMTD and MP	"Paste and peel off" Au NPs	0.24 and 2.6 ng/cm^2	46
TMTD and MP	MoS_2@Ag nanoflower	1.3×10^{-6} and 1.8×10^{-6} mg/mL	This work

TOC

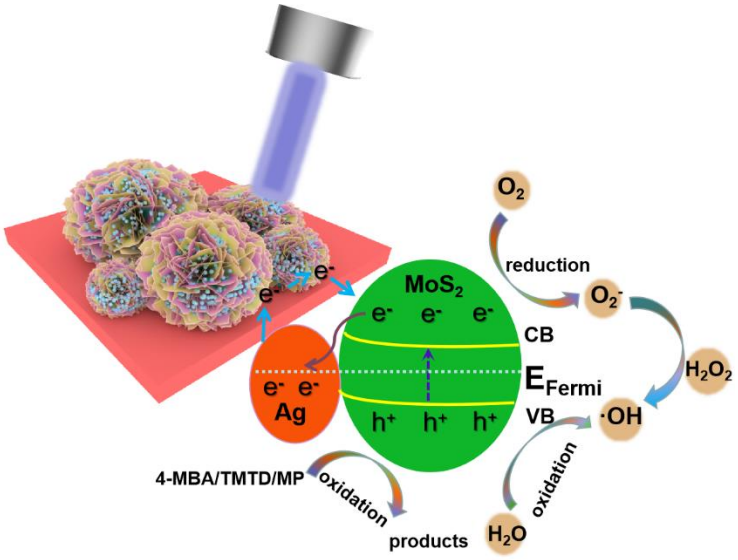
O_2
reduction
O_2^-
MoS_2
e⁻ e⁻ e⁻
CB
E_{Fermi}
VB
h⁺ h⁺ h⁺
H_2O_2
·OH
oxidation
H_2O
e⁻ e⁻
Ag
e⁻
e⁻
4-MBA/TMTD/MP
oxidation
products